Airborne Docking

Rigid airborne docking between a fixed-wing UAV and an over-actuated multicopter

Jonathas Laffita van den Hove

Delft University of Technology

TU Delft

Airborne Docking

Rigid airborne docking between a fixed-wing UAV and an over-actuated multicopter

by

Jonathas Laffita van den Hove

Student number: 4431693

Exam Committee:

Dr. E. J. J. Smeur,	TU Delft
Dr. G.C.H.E. de Croon	TU Delft
Ir. B.D.W. Remes	TU Delft
Dr. A. Bombelli	TU Delft

Cover: Shot by Jonathas Laffita at the OJF, Aerospace faculty

TU Delft

Preface

I am happy to present my master's Thesis report, which ends my journey as a student in Delft. I am very thankful for the inspiring people I have met along the way and the knowledge that TU Delft has given me.

I would like to express my sincere gratitude to my supervisors, Bart Remes and Ewoud Smeur for their guidance and perseverance throughout my thesis journey. I would also like to thank Alessandro Mancinelli for his help with the Rpi-paparazzi communications, as well as Tom Suys, Erik Dedding, and Ahmed Tork for their help with the wind tunnel experiments. Finally, I would like to thank Mohamed Khalifa and Elida Barrios for their continuous encouragement.

In this Thesis, a concept for rigid airborne docking is put forward and a proof of concept is put to the test. I believe the concept presented has potential and is worth future development. I thank the reader for his interest in this Master's Thesis and hope that it can be used as a starting step for future developments.

Jonathas Laffita van den Hove
Delft, June 2023

Contents

1

Introduction

1.1. Motivation

Unmanned aerial vehicles have seen a rapid increase in use and development over the last decade. Apart from being used extensively for aerial photography and videography, they are now being explored for package delivery, agriculture, industrial inspections, rescue operations, environmental monitoring, mapping, and surveying[1]. For these missions, it is more common to use rotorcraft as opposed to fixed-wing aircraft, due to their capability of vertical takeoff and landing (VTOL) as well as hovering. While the need to hover may be a pre-requisite for some missions, it is not a requirement for all of them. Of course being able to takeoff and land vertically is beneficial, but it comes at a cost: flight endurance and range[2].

Hybrid UAVs combine VTOL capability with a wing for efficient forward flight, but they tend to be harder to control during hovering, due to the wing surface that can catch gusts, and they are less efficient during cruise flight due to the extra systems needed to facilitate hovering. That is where the need for airborne docking comes in. A rotorcraft could be used to assist in the takeoff and landing of the fixed-wing aircraft, such that the fixed-wing can be optimized for efficient flight while retaining the VTOL capability.

The concept proposed involves an overactuated multicopter to approach the fixed-wing aircraft from below to avoid disturbing the airflow over the aircraft's aerodynamic surfaces and dock onto it rigidly using electromagnets. To achieve the precise relative control desired for the docking maneuver, three additional motors will be added to the multi-copter: two laterally and one longitudinally. This will also allow to decouple position from attitude.

This paper focuses on the rotorcraft and the contributions are as follows: A relative control and guidance strategy for the overactuated platform will be put forward, and validated by performing wind tunnel experiments. In these, docking and separation maneuvers will be done with a target at fixedwing airspeeds. The use of electromagnets as a docking system will also be put to the test. To achieve this feat, a relative sensing method that involves IR LEDs in combination with retroreflective ArUco markers will be used.

1.2. Research Question(s)

After having carried out the literature review, it became clear that there is a need for rigid airborne docking, and while the advancements in both hardware and control methods seem sufficient to make it a reality, it has never been demonstrated in practice. The work aims to change that through a proof of concept in which an overactuated multi-copter approaches the fixed-wing aircraft from below to avoid disturbing the airflow over the aircraft's aerodynamic surfaces and docks onto it rigidly using electromagnets. To achieve the precise relative control desired for the docking maneuver, three additional motors will be added to the multi- copter: two laterally and one longitudinally. This will also allow to decouple position from attitude. The main research question is then:

Is the use of electromagnets and the use of an overactuated multicopter, a viable solution for rigid airborne docking between a fixedwing UAV and a rotorcraft?

Since the above question can be answered with a simple "yes", "no" or "it depends", further subquestions are necessary to arrive at a more precise and complete response:

- **What degree of position control can be achieved with the overactuated multicopter?**

  In order to rigidly dock to a mechanism like an electromagnet, precise relative control, and attitude must be achieved. The dynamics achievable by the multicopter must therefore be evaluated.
- **Are electromagnets a viable solution for airborne docking of UAVs?**

  The use of electromagnets as a docking solution must be evaluated. The degree of precision needed to achieve a successful docking maneuver must first be determined. Then, the magnet size needed to ensure a secure connection must be evaluated. Finally, the effect of using electromagnets on other subsystems must be investigated.
- **What relative sensing methods are needed to achieve successful airborne docking?**

  Even if the overactuated rotorcraft has the ability to control its position impeccably, the relative precision accuracy is limited by the relative sensing accuracy. Different sensing methods must therefore be considered, and a suitable method should be chosen to make a proof of concept.

1.3. Research Objective

Given the multifaceted problem that is airborne docking, the goal of the work done can be seen as a stepping stone toward a successful outdoor experiment. The main goal of this thesis is therefore to **Successfully dock and separate with a fixed-wing aircraft at airspeeds of** $14\mathbf{m/s}$ **or above**

The sub-goals are:

- Develop and build the overactuated UAV used in the experiments
- Implement a control method to achieve precise and aggressive control
- Design a relative guidance algorithm
- Implement a relative sensing method

1.4. Structure of the document

After this introduction, puts forward the research to be carried out, the report is split into two main parts. Part I is the scientific paper written from the work that was done. This paper can be read by itself and encompasses the main contributions of this Master's thesis. The paper is divided into 5 sections: In the introduction, the problem statement is revealed, relevant work is discussed, and the contributions of the paper are put forward. The second section focuses on the control of the overactuated multicopter. In the third section, the relative sensing method is explained. The fourth section shows the wind tunnel experiment setup as well as the results. Finally, a small conclusion is presented in the last section. Right after the scientific paper, the details that could not fit within the page limits of the scientific paper are put forward, including any additional remarks and recommendations. In Part II of the thesis report, the reader can find the literature review.

Part I

Scientific Article

Rigid Airborne docking between a fixed-wing UAV and an over-actuated multicopter

J.J.E. Laffita van den Hove*, E.J.J. Smeur, and B.D.W. Remes
Delft University of Technology, Faculty of Aerospace Engineering, Kluyverweg 1, Delft, Zuid-Holland, The Netherlands

ABSTRACT

Fixed-wing aircraft fly longer, faster, and further than rotorcraft, but cannot take off or land vertically. Hybrid drones combine VTOL with a wing for forward flight, but the hovering system generally makes them less efficient than a pure fixed-wing. We propose an alternative, in which a rotorcraft is used to assist the fixed-wing UAV with the VTOL portions of the flight. This paper takes the first steps towards this alternative by developing and testing an overactuated rotorcraft that can autonomously dock onto a target at fixed-wing velocities. The control system uses Incremental Non-Linear Dynamic Inversion Control (INDI) to achieve linear accelerations with lateral and longitudinal motors, enabling robust horizontal control independent of attitude. A relative guidance algorithm for the docking approach path is presented, along with a vision sensing approach using ArUco markers and IR LEDs. Successful docking and separation were achieved in the wind tunnel at speeds of up to 15m/s.

1 INTRODUCTION

Unmanned aerial vehicles have seen a rapid increase in use and development over the last decade[1]. For most uses, it is more common to use rotorcraft as opposed to fixed-wing aircraft, due to their capability of vertical takeoff and landing (VTOL) as well as hovering. While the need to hover may be a pre-requisite for some missions, it is not a requirement for all of them. Of course being able to takeoff and land vertically is beneficial, but it comes at the cost of flight endurance and range[2].

Hybrid UAVs combine VTOL capability with a wing for efficient forward flight, but they tend to be harder to control during hovering, due to the wing surface that can catch gusts, and they are less efficient during cruise flight due to the extra systems needed to facilitate hovering. That is where the need for airborne docking comes in. A rotorcraft could be used to assist in the takeoff and landing of the fixed-wing aircraft, such that the fixed-wing can be optimized for efficient flight while retaining the VTOL capability. The author proposes the use of an overactuated rotorcraft with electromagnets as the docking solution.

1.1 Relevant work

Airborne docking systems can be categorized as rigid or non-rigid, the former being systems for which the docking apparatus is comprised of rigid members while the latter utilizes flexible materials that can easily deform such as ropes or nets.

Various non-rigid docking solutions have been developed to recover fixed-wing UAVs without a landing strip. One approach involves arresting systems using horizontal or vertical ropes in combination with a hooking mechanism at the tail or wingtips [3, 4, 5]. This can be achieved using a multicopter, a crane, or a kite dragged by a moving vehicle. Although these approaches require infrastructure and manual recovery, they benefit from requiring low precise control.

A true airborne variation of the aforementioned solution is presented in [6], where two multicopters are used to carry the arresting rope. The rotorcrafts used RTK GPS to position themselves in the right position for successful capture. The recovery margins are dictated by the length of the hook line and horizontal catch line, which can easily be increased, making this recovery method very robust. The same method was used with a net in [7], which was experimentally verified [8]. However, the net method had drawbacks including increased weight and wind influence, as well as a higher risk of equipment damage compared to single hook alternatives.

Current systems that would allow for docking and separation mid-flight have been in the form of a probe and drogue approach. Extensive research has gone into Air-to-Air refueling for large aircraft and are summarized in [9]. In the world of smaller UAVs, Wilson successfully had a fixed-wing UAV to autonomously dock with a drogue towed by another UAV[10]. To improve the estimation of the relative distance between the UAVs, his system fuses direct vehicle-to-vehicle observations in the state estimates. Dynetics successfully recovered an X-61A aircraft using a drogue towed from a C130 Aircraft[11].

With regards to rigid solutions, Steven Lukow aimed to design and fabricate a prototype of an autonomous multirotor drone that can dock onto a larger fixed-wing drone for Mars exploration [12]. Electromagnetic coils mounted on the fixed-wing drone were used to form a connection with two neodymium magnets mounted on the top of the multirotor. A demonstration was not shown. In [13] the author uses a

*Email address(es): jonathaslvdh@gmail.com

marker on an unmanned ground vehicle (UGV), such that a fixed-wing UAV could recognize the target and relative pose, and finally land on it. Tests were done at very slow speeds, and the system became unstable at higher speeds. In [14] the same setup is used, but this time with a gimballed camera that points towards the received location of the ground vehicle. Successful landings were achieved on a high-speed ground vehicle traveling at 50km/h.

Clearly, there have been many advancements toward airborne docking. However, there is no instance of it being done between rotorcraft and a fixed-wing UAV at forward flight velocities.

1.2 Contributions

The concept proposed involves an overactuated multicopter to approach the fixed-wing aircraft from below to avoid disturbing the airflow over the aircraft's aerodynamic surfaces and dock onto it rigidly using electromagnets. To achieve the precise relative control desired for the docking maneuver, three additional motors will be added to the multicopter: two laterally and one longitudinally. This will also allow to decouple position from attitude.

This paper focuses on the rotorcraft and the contributions are as follows: A relative control and guidance strategy for the overactuated platform will be put forward, and validated by performing wind tunnel experiments. In these, docking and separation maneuvers will be done with a target at fixed-wing airspeeds. The use of electromagnets as a docking system will also be put to the test. To achieve this feat, a relative sensing method that involves IR LEDs in combination with retroreflective ArUco markers will be used. An illustration of the desired system can be seen in Figure 1.

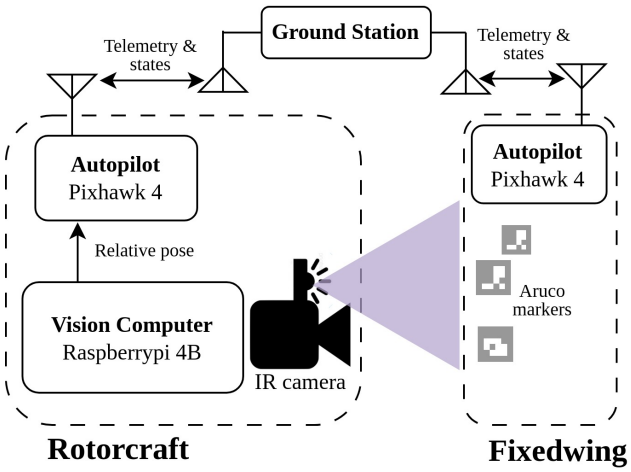

Figure 1: System Architecture.

2 CONTROL

2.1 INDI for linear accelerations

Traditional rotorcraft need to adjust the attitude in order to control their position. This is identified as a potential problem in the docking process. To be able to control the position of the rotorcraft independently of attitude, one back propeller and two side propellers are used, resulting in an over-actuated platform, as can be seen in Figure 2. To simplify the control problem, the four propellers facing downward will be used for attitude control and the generation of vertical lift, while the 3 side propellers will be used for horizontal position control. The attitude of the drone is controlled with INDI [15]. It is assumed that the moments resulting from the lateral-acting motors are negligible, and any effect they do have will be treated as a disturbance. For position control, a variation of [16] will be implemented, where the side actuation will be used instead of the attitude angle to achieve horizontal control. The two reference frames that will be used in this section are the body frame and the North, East Down (NED) frame, which is assumed to be an inertial frame. The body frame is depicted in Figure 2 and is denoted by subscript B. The NED frame, indicated with subscript N, has its axes pointing North, East, and Down, and its origin is fixed to a point on earth of choice.

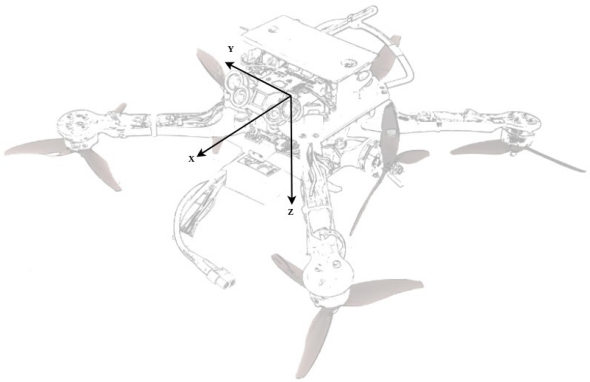

Figure 2: Body reference Frame.

The position dynamics of the aircraft in the NED frame is given by Newton's second law of motion:

$$\ddot{\xi} = g + \frac{1}{m}F(\dot{\xi}, w) + \frac{1}{m}T_N(\eta, T_B), \tag{1}$$

where ξ is the position of the vehicle, g is the gravity vector, F is the sum of aerodynamic forces acting on the airframe, and T is the thrust vector, which contrary to other conventional multicopters does not only act through the z-axis of the vehicle.

The aerodynamic force is a function of aircraft velocity $\dot{\xi}$ and wind vector w, and the thrust vector is dependent on the attitude of the drone $\eta = \begin{bmatrix}\phi & \theta & \psi\end{bmatrix}^T$, expressed in Euler

angles with the traditional ZYX rotation order, as well as the total thrust T_B in the body frame. Due to the side motors, the vehicle can produce thrust along all axes, as opposed to only along the Z axis. T_N is given by:

$$\begin{aligned} T_N(\eta, T_B) &= M_{NB}(\eta) T_B \\ &= \begin{bmatrix} c\psi c\theta & c\psi s\theta s\phi - s\psi s\phi & s\psi s\theta + c\phi s\theta c\phi \\ s\psi c\theta & c\psi s\theta s\phi & s\psi s\theta c\phi - c\psi s\phi \\ -s\theta & c\theta s\phi & c\theta c\phi \end{bmatrix} \cdot \begin{bmatrix} T_{B_X} \\ T_{B_Y} \\ T_{B_Z} \end{bmatrix}, \end{aligned} \quad (2)$$

where the sine and cosine are abbreviated by the letters s and c respectively. Now a first order Tailor expansion can be done on Equation 1 to obtain Equation 3:

$$\begin{aligned} \ddot{\xi} = {} & g + \tfrac{1}{m} F(\dot{\xi_0}, w_0) + \tfrac{1}{m} T_N(\eta_0, T_{B_0}) \\ & + \tfrac{\sigma}{\sigma \dot{\eta}} \tfrac{1}{m} F(\dot{\xi}, w_0)|_{\dot{\eta}=\dot{\eta}_0} (\dot{\eta} - \dot{\eta}_0) \\ & + \tfrac{\sigma}{\sigma w} \tfrac{1}{m} F(\dot{\xi}_0, w)|_{w=w_0} (w - w_0) \\ & + \tfrac{\sigma}{\sigma \phi} \tfrac{1}{m} T_N(\phi, \theta_0, \psi_0, T_{BX_0}, T_{BY_0}, T_{BZ_0})|_{\phi=\phi_0} (\phi - \phi_0) \\ & + \tfrac{\sigma}{\sigma \theta} \tfrac{1}{m} T_N(\phi_0, \theta, \psi_0, T_{BX_0}, T_{BY_0}, T_{BZ_0})|_{\theta=\theta_0} (\theta - \theta_0) \\ & + \tfrac{\sigma}{\sigma \psi} \tfrac{1}{m} T_N(\phi_0, \theta_0, \psi, T_{BX_0}, T_{BY_0}, T_{BZ_0})|_{\psi=\psi_0} (\psi - \psi_0) \\ & + \tfrac{\sigma}{\sigma T_{BX}} \tfrac{1}{m} T_N(\phi_0, \theta_0, \psi_0, T_{BX_0}, T_{BY_0}, T_{BZ_0})|_{T_{BX}=T_{BX_0}} (T_{BX} - T_{BX_0}) \\ & + \tfrac{\sigma}{\sigma T_{BY}} \tfrac{1}{m} T_N(\phi_0, \theta_0, \psi_0, T_{BX_0}, T_{BY_0}, T_{BZ_0})|_{T_{BY}=T_{BY_0}} (T_{BY} - T_{BY_0}) \\ & + \tfrac{\sigma}{\sigma T_{BZ}} \tfrac{1}{m} T_N(\phi_0, \theta_0, \psi_0, T_{BX_0}, T_{BY_0}, T_{BZ_0})|_{T_{BZ}=T_{BZ_0}} (T_{BZ} - T_{BZ_0}) \end{aligned} \quad (3)$$

The first terms $g + \frac{1}{m} F(\dot{\xi}_0, w_0) + \frac{1}{m} T_N(\eta_0, T_{B_0})$ can be simplified to the acceleration at the previous time step. This can be obtained by using the IMU acceleration readings and rotating them to the NED frame. The gravitational acceleration must then be added to that. There is no good estimate for the partial derivatives of $F(\dot{\xi}, w)$ as developing an aerodynamic model would be very time-consuming and the changes in the wind are hard to obtain. These two terms will therefore be taken as 0. This does not mean these forces will be neglected, but just included in the term $\ddot{\xi}_0$. The partial derivatives of ϕ, θ, and ψ will also be neglected, as for the time being, there will not be any aggressive attitude commands in the airborne docking maneuver. Implementation of these terms is considered future work.

Equation 3 can now be rewritten into:

$$\ddot{\xi} = \ddot{\xi_0} + \frac{1}{m} G(\eta_0, T_{B0})(u - u_0), \quad (4)$$

where $\mathbf{u} = \begin{bmatrix} T_{BX} & T_{BY} & T_{BZ} \end{bmatrix}$ and

$$G(\eta_0, T_{B0}) = \begin{bmatrix} c\psi c\theta & c\psi s\theta s\phi - s\psi s\phi & s\psi s\theta + c\phi s\theta c\phi \\ s\psi c\theta & c\psi s\theta s\phi & s\psi s\theta c\phi - c\psi s\phi \\ -s\theta & c\theta s\phi & c\theta c\phi \end{bmatrix}, \quad (5)$$

which is referred to as the control effectiveness matrix.

The accelerometer measurements obtained to determine $\ddot{\xi}_0$ are normally very noisy due to vibrations stemming from the rotating propellers. They are therefore filtered using a second order low pass filter. Since a filter introduces a delay, all other terms with subscript 0 must therefore also be filtered with the same filter. Now Equation 4 can be inverted to obtain:

$$u_c = u_f + mG^{-1}(\eta_0, T_0)(v_{\ddot{\xi}} - \ddot{\xi}_f). \quad (6)$$

Note that all values that are filtered are denoted with a subscript f. The virtual control $v_{\ddot{\xi}}$ is the desired acceleration of the vehicle and u_c is the resulting control output. The control block diagram can be seen in Figure 3.

2.1.1 Thrust estimation

The actuator dynamics can be modeled using the 1st order system shown in Equation 7

$$A(z) = \frac{\alpha}{z - (1 - \alpha)} \quad (7)$$

where α was estimated to be 0.069 at 500Hz.

The vertical control increment $\widetilde{T}_{BZ}$ is controlled through the four down-facing propellers and is passed to the inner attitude loop. The way this thrust increment is used is further described in [15]. Since the over-actuated multicopter is designed to be flying forward at fixed-wing aircraft speeds, there will always be an aerodynamic force acting in the negative X_B direction. One motor acting forwards is therefore sufficient for longitudinal control. At lower speeds, where aerodynamic drag is not significant for longitudinal control, the two aircraft are already docked, so precise control is not needed. In this case, reversing the direction of rotation of the propeller is sufficient for longitudinal control, albeit using different gains due to the slower dynamics. For lateral control, two motors facing away from each other are used. The PWM command to each lateral motor is:

$$T_{L_c} = T_{min} \leq T_{base} + T_{BY_c} \leq T_{max}, \quad (8)$$

$$T_{R_c} = T_{min} \leq T_{base} - T_{BY_c} \leq T_{max} \quad (9)$$

Where T_{L_c} and T_{R_c} are the command to the left and right motor respectively, T_{base} is the baseline thrust of both motors and T_{BY_c} is the commanded side thrust. The total side thrust T_{B_Y} then results from subtracting the thrust of the left and right motor.

A quadratic relationship governs the rotational speed of the propellers and thrust. That means that the thrust effectiveness ($\frac{dT}{dT_c}$) of each motor increases linearly with its rotational speed. In the context of the side propellers, increasing T_{BY_c} will lead to an increase in the thrust effectiveness of the left motor. However, it will also lead to an equal decrease in the thrust effectiveness of the right motor. The overall effectiveness of the lateral command $\frac{da_y}{dT_{BY_c}}$ will therefore remain constant as long as $T_{BY_c} \leq min(T_{base} - T_{min}, T_{max} - T_{base})$. Beyond that, the thrust effectiveness of one motor will increase more than the other would decrease, and therefore the assumption that the effectiveness remains constant does not hold anymore. It will then change linearly for higher lateral commands.

For the longitudinal thrust, the control effectiveness of the pusher motor was determined at an airspeed of $12m/s$. Since the effectiveness changes with the propeller RPM, flying at higher or lower speeds tends to give an oscillatory response.

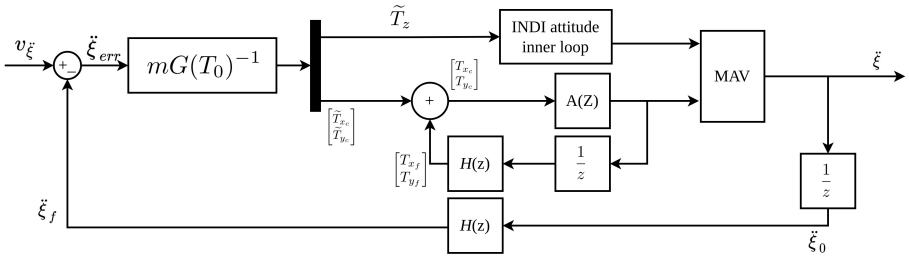

Figure 3: Control diagram of the guidance loop

In Figure 4, we can appreciate the vehicle response to lateral acceleration commands at various roll angles. The acceleration is tracked well, except for when saturation occurs due to a large acceleration command in combination with a roll angle.

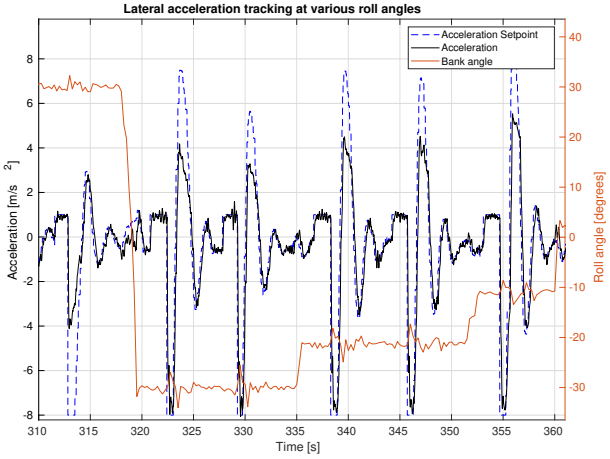

Figure 4: Lateral acceleration tracking at varying roll angles.

2.2 *Position Control*

In subsection 2.1 the way INDI control is used to achieve linear accelerations is put forward. Now position must be controlled by commanding desired accelerations to the INDI controller in the NED frame. To do this, a simple cascaded proportional controller is used and can be observed in Figure 6. The commanded relative velocity is $\dot{\xi}_{ref} = \xi_{ref} \cdot K_p$ and the acceleration $v_{\ddot{\xi}} = \dot{\xi}_{ref} \cdot K_{\dot{\xi}}$.Due to the physical limitations of the aircraft, $\dot{\xi}_{ref}$ and $v_{\ddot{\xi}}$ are bounded to 15m/s and 6m/s^2 respectively. The gains can be tuned such that the response is sufficiently fast, while preventing significant overshoot. In Figure 5 we can see a response to a position step command 2.75m to the right. This was achieved with a velocity gain of 2.0 ms^{-2}/(ms^{-1}) and a position gain of 3.0 ms^{-1}/(m^{-1}).

2.3 *setpoint generation*

Now that the position of the rotorcraft can be controlled, the setpoint generation to achieve successful docking is considered. Note that the position and velocity errors now become relative errors, but the controller performance should stay unaffected if the fixed-wing drone flies at a constant speed. Values will be in the NED frame, with the fixed-wing UAV in the origin. As mentioned before, the rotorcraft must first reach a pre-docked setpoint, after which it starts the approach. This approach path can be visualized in Figure 7. The rotorcraft position reference will advance from the pre-docked position P_{pd} to the docked position P_d gradually until docking is achieved. To ensure that the approach leads to a successful docking attempt, the reference will only advance if the rotorcraft error to its target is within a certain horizontal distance threshold. This threshold is made linearly smaller as the distance to the aircraft is decreased. That is why the two dashed lines seen in Figure 7 get closer to each other. Algorithm 1 shows the approach logic.

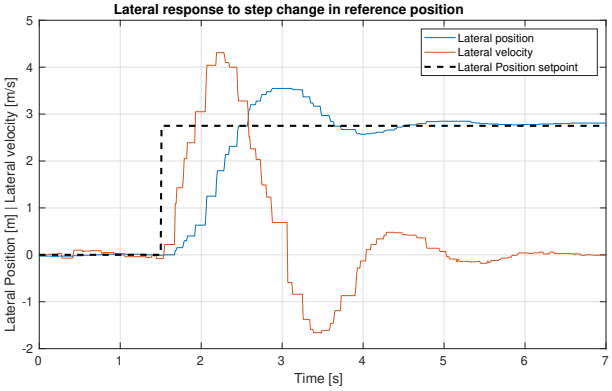

Figure 5: Position response to a step input.

The reference position is given by:

$$\xi_{ref} = \xi_{fw} + \begin{bmatrix} \cos\psi_{fw} & -\sin\psi_{fw} & 0 \\ \sin\psi_{fw} & \cos\psi_{fw} & 0 \\ 0 & 0 & 1 \end{bmatrix} \cdot \left(P_{pd} + K_{adv} \cdot (P_d - P_{pd})\right) , \tag{10}$$

Where ξ_{fw} is the fixed-wing NED position and K_{adv} is a number from 0 to 1 that dictates, where along the path from P_{pd} to P_d the position reference should be. P_{pd} and P_d are a predetermined position with respect to the aircraft, in which the reference frame is the NED frame rotated along the Z axis by the fixed-wing aircraft heading ψ_{fw}. X will therefore point

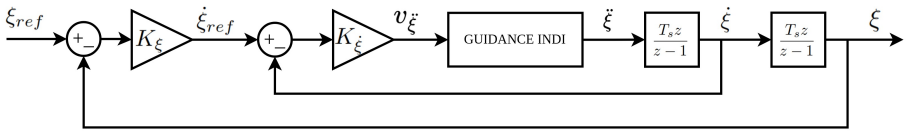

Figure 6: Position control loop

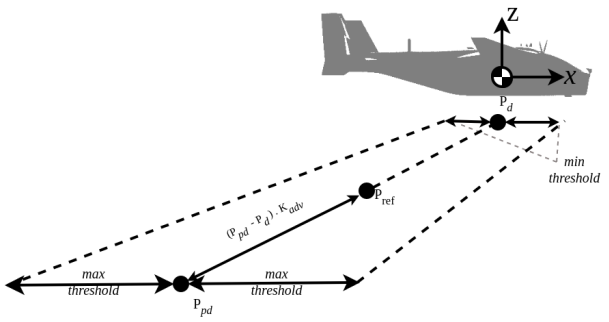

Figure 7: Setpoint generation.

in the same direction as the fixed-wing aircraft, and the point $\begin{bmatrix}2 & 0 & -5\end{bmatrix}^T$ is 2 meters below, and 5 meters behind the aircraft. Note that the reference position does not change due to a pitch or roll change of the fixed-wing, but is affected by a change in its heading.

In the docking sequence, the rotorcraft first reaches the *pre-docked* position. Then, the setpoint moves along the approach path towards the *Docked position*. At every iteration of the setpoint generation module, which is running at 100 Hz, the rotorcraft's horizontal distance to the approach centerline is evaluated, and if it is within the error threshold, then the reference progresses forward. If the aircraft is outside the error threshold, then the reference is moved backward. The amount by which the setpoint progresses along that line is defined by the value k_{adv}.

The error threshold E_{th} is also scaled by k_{adv}, to allow for more error when further away from the fixed-wing. During the experiments, this error threshold decreases linearly from 0.4m at the pre-docked setpoint, to 0.1m at the docked setpoint.

To avoid rapid changes in the reference position due to a momentary change in the heading of the fixed-wing, ψ_{fw} is first filtered with a low pass filter. The commanded heading of the rotorcraft is also set to ψ_{fw}.

2.4 switching between GPS and vision

To achieve successful docking, the relative position should be accurately estimated. This could be potentially possible with RTK GPS, but in order not to rely on an RTK fix, computer vision is used to augment the GPS. The pre-docked setpoint is, therefore, a point where the two aircraft can be positioned in a safe, yet close enough distance so that the vision system is operative. Once the vision estimates have a good confidence, the relative positioning is done purely on vision. During the approach, vision dropouts can occur. To avoid dropping back to GPS and therefore to the pre-docked setpoint straight away, a buffer is implemented, as can be seen in algorithm 1 where the *Vision confidence* decreases with every loop iteration during a dropout, eventually reaching 0 and forcing the fallback to GPS. While in the dropout, the relative position estimate remains the same, and therefore, the relative acceleration command also remains the same.

Input: Detected markers, position estimate (vision & GPS
Output: updated Setpoint
Setpoint ← predocked Setpoint;
while *in flight* **do**
  if *markers detected* > 2 **then**
    increase vision confidence;
  else
    decrease vision confidence;
  end
  if *vision confidence* $>$ *threshold* **then**
    `// Use vision`
    if *horizontal error* $<$ *threshold* **then**
      move Setpoint forward;
    else
      move Setpoint backwards;
    end
  else
    `// Use GPS`
    Setpoint ← predocked Setpoint;
  end
end

Algorithm 1: Setpoint generation at module frequency (100hZ)

3 RELATIVE SENSING

To implement the developed control system, the relative position, relative heading, and relative velocity of the two vehicles must be estimated accurately. For the proposed rigid docking apparatus to work the position accuracy must be at least 5cm. To do so, GPS and a monocular camera will be used in cooperation. The GPS measurements, which can achieve a relative position accuracy lower than 2 meters [17], will be used to reach a formation within the range of the vision system. Once within range, the more accurate vision system estimates the relative pose and its derivative to perform the docking maneuver.

3.1 Vision

To estimate the aircraft's relative pose using a monocular camera, a Perspective-N-Point problem is solved using OpenCV. The process involves detecting known points on the aircraft and finding the transformation matrix which mini-

mizes the re-projection error between the 2D image points and the 3D object points. In [18] the authors used the corners of ArUco markers placed on a drone to estimate relative pose. In [10] Wilson used a known pattern of IR LEDs that could be used as object points and could be detected at a distance of up to $30m$ away.

In this proof of concept, we use a combination of both implementations; ArUco markers will be used for their already-implemented detection algorithms, and the markers are made of IR reflective tape (3M High-Reflex-Tape type 7610). The rotorcraft is equipped with 940nm IR LEDs, and a band-pass filter around the same frequency is used on the camera to minimize any unwanted light. This makes the markers clearly visible in a wide range of lighting conditions.

A comparison between a regular black and white marker and the proposed retroreflective markers is shown in Figure 8. The retroreflective marker offers better visibility and distinct edges, enhancing detection. Selection of the reflective tape is critical to prevent overexposure caused by the IR LEDs. The corner points of the ArUco markers are used as the object points. To ensure marker detection at a range, a combination of small and large ArUco markers is placed around the aircraft. This approach increases the scope of the marker detection [18].

The vision computer used is a RaspberryPi 4B that is constantly running three threads. The first thread processes the camera feed and estimates the relative pose (translation vector + rotation vector). The second thread uses the same feed to calculate the optical flow. The third thread sends the estimated relative distance in the body frame, the optical flow, and the relative heading to the autopilot through a serial interface. With this setup, the relative pose is estimated at an average of $32Hz$ at a resolution of 640 x 480 pixels.

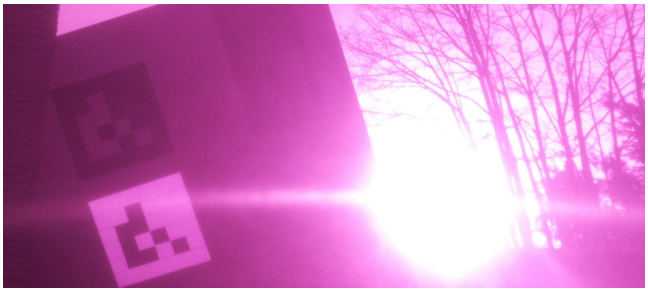

Figure 8: Conventional ArUco marker compared to proposed marker when backlit.

3.2 Calculating the relative state

After the visible markers have been detected, the 4 corner points of each of them are known. Given that the marker ID of each of these points are known, and the exact location where these markers are placed on the UAV is also known, we now have a series of (2D) image points with their respective (3D) object points. This data can be directly used in the SolvePnP() function in OpenCV. The estimated translation vector T_{vec} obtained can then be used to find the relative NED position using:

$$\xi_{\text{rel}} = -R_{NB} R_\delta T_{vec}, \tag{11}$$

where R_{NB} is the rotation vector from the Body frame to the NED frame, and R_δ is the camera offset, which can be adjusted by comparing the estimated relative position to the true relative position. R_δ can be seen as the rotation matrix from the camera frame to the body frame.

At any point in time, the rotation vector from the body frame to the NED frame is calculated using the estimated attitude of the rotorcraft. The relative heading ψ_{rel} can be calculated by applying the Rodrigues rotation formula to the obtained rotation vector. The estimated fixed-wing heading ψ_{fw} then becomes:

$$\psi_{fw} = \psi_{rot} + \psi_{rel}\,, \tag{12}$$

where ψ_{rot} is the heading of the rotorcraft. This way, the final approach can take place without communication between the vehicles.

The vision distance estimates are compared with measurements of an external infrared tracking system during several docking attempts. It was observed that the vision error decreases as the aircraft approaches the target. After compensating for camera offset angles, which are seen as constant errors that linearly increased with distance, the absolute error of the vision system is shown in Figure 9. As the rotorcraft approaches the target, the error decreases to below 5cm.

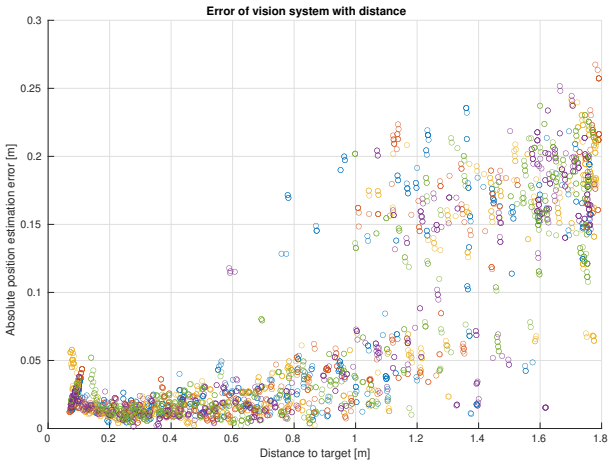

Figure 9: Vision position estimation error with distance.

4 Wind Tunnel Tests

As a stepping stone towards outdoor flight, wind tunnel tests were carried out. This allowed us to validate that the over-actuated platform can indeed serve the intended purpose in forward flight, at fixed-wing UAV velocities. The wind tunnel setup allows to keep the follower drone tethered at all

times and track its position at mm accuracy, allowing it to be tuned easily, without the risk of crashing.

The facility used is the Open Jet Facility of the TU Delft Aerospace Engineering faculty. It has a cross-section of $2.85m$ by $2.85m$ at the test area and can produce wind speeds of up to $30m/s$. The test setup can be seen in Figure 10. To simulate the fixed-wing aircraft, a cruciform beam is attached to the wind-tunnel roof, at the throat, allowing to maximize the approach path size. As can be seen in the image, the follower can be tethered to the roof with a rope and is operated by an assistant in order to always keep the rope slack, without allowing it to get tangled into the propellers. The facility contains a motion capture system called *Optitrack*, which can track position and attitude at mm accuracy and relay it to the UAVs via the ground station.

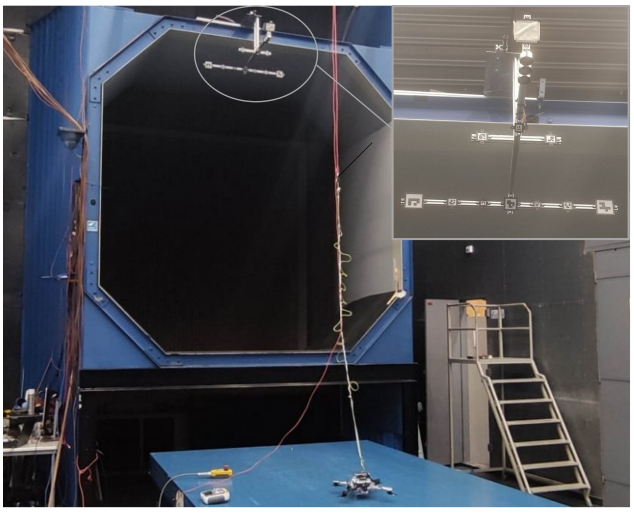

Figure 10: Wind tunnel test setup

4.1 *fixed-wing aircraft*

The fixed-wing aircraft will be simulated by a cruciform beam and can be seen in Figure 10. Given that most aircraft are of fuselage + wing configuration, that was the shape used. The width and length are both $180mm$. Thirteen Aruco markers were placed around the "*airframe*", varying in width, ranging from $2cm$ to $10cm$. This enables the markers to be seen from further away, while still keeping full markers in view when in proximity. Three $25kg$ pot electromagnets are aligned to form the docking point. In future work, they will be spaced to ensure an exact docking position. The three electromagnets are powered with a 3-cell LiPO battery and can be turned off with a momentary-push button. The electromagnets can therefore be powered off to be able to simulate separation mid-flight.

4.2 *Rotorcraft*

The manufactured rotorcraft can be seen in Figure 2 and its hardware characteristics are tabulated in Table 1. This drone is an adaptation of an F350 drone frame, where the top and bottom plate are re-designed, and 3D printed to accommodate the three lateral motors. A longer landing gear was also made to allow the lateral rotors to spin without hitting the ground. Due to the lateral motors, stronger vibration can now be expected around all three axes. Passive damping is therefore included, where the camera and the flight controller are both suspended on a damped rubber platform.

A flat metal plate is installed that will attach to the electromagnets. A thickness of $3mm$ is chosen as it is a good compromise between pull force and mass. Finally, to avoid the tether from getting tangled into the back propeller, a simple propeller guard was included. Note that the four downfacing propellers are in pusher configuration, to assure the necessary clearance for docking.

Table 1: Follower platform characteristics

Take-off weight	1050 [g]
Frame:	Modified F350 plastic drone frame
Motors:	7 x Readytosky 2205 2700kV
ESCs:	Racestar V2 30A
Propellers:	GemFam 5146
Flight controller	Pixhawk 4
On_board computer	Raspberry-pi 4B
Camera	Rasberry-pi v2 noIR
Telemetry	SIK telemetry module
Flight software	Paparazzi

4.3 *Experiment setup and results*

Various tests were carried out to assess the feasibility and discover any challenges of the concept proposed. Three primary questions had to be answered. First, whether the platform can fly at forward velocities matching a fixed-wing aircraft while maintaining level and stable flight. Second, evaluate whether precise enough relative control can be achieved for rigid airborne docking to be feasible. And lastly, verify that the proposed docking method is viable and whether accidental detachments would not take place at these airspeeds.

To answer the first question, the aircraft was flown in the wind tunnel at a fixed position, while airspeed was incrementally increased up to 17.2m/s, at which speed the pusher propeller was saturated. The aircraft remained level with attitude deviations not surpassing 3^o in all axes and its position within 5cm. The relative position tracking capabilities were not affected significantly when flying a flag in front of the aircraft at $14m/s$. Footage of this can be seen on Youtube[1].

The second question is answered by performing the approach and docking procedure in the wind tunnel, starting from the pre-docked position. The aircraft then autonomously approaches the target and docks onto the simulated fixed-wing aircraft. As soon as the operator sees that docking is successful, he turns off the motors and resets the desired po-

[1] https://www.youtube.com/playlist?list=PLGTkt2QO0hTnYZ0R1N5Mrnp9tA1FefnFx

sition to the pre-docked setpoint. When ready, the operator arms the aircraft and pushes the button that disables the electromagnets. The over-actuated platform then returns to the pre-docked setpoint aggressively. This sequence can be seen in Figure 11. The security tether is always left slack.

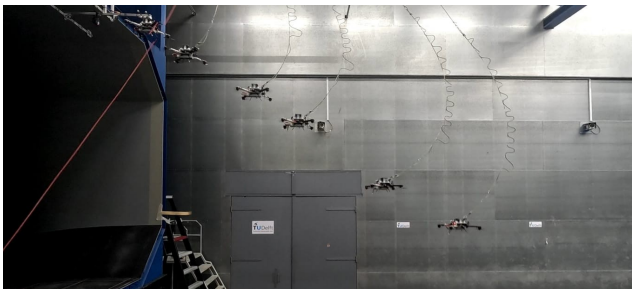

Figure 11: Approach sequence.

The approach path for 5 consecutive docking maneuvers at 13m/s can be seen in Figure 12. The rotorcraft uses Optitrack to reach the pre-docked setpoint, and from there, once the vision confidence is above the threshold, the docking procedure is started with the vision measurements. In these tests, the relative velocity is still obtained from Optitrack. Due to the markers being too small, the pre-docked setpoint had to be moved closer to -1.6m behind and 0.8m below the target. This problem can be mitigated by using larger markers, or increasing the resolution of the camera.

In the figure, the two dark dashed lines are the error threshold around the center line at any given position. This seems like a very narrow approach, but only the horizontal error to the current setpoint is taken into account for the advancement of the desired position setpoint. In fact, we see that the 5 approaches follow almost an identical path that is not through the center line. This is because there is no feedforward control in place to make the rotorcraft exactly track the setpoint, and only the error controller makes the vehicle follow the setpoint, which is advancing faster than what the error controller can keep up with. The follower aircraft is effectively trailing the setpoint by the error threshold. For this specific scenario, in which the leader is not moving and there is almost no turbulence, it makes the approach very smooth.

In the same figure, the setpoint position can be seen as well as the error threshold at that specific moment for one of the approaches. An animation of this is also available on youtube. We can see that indeed, the aircraft is trailing behind the setpoint by the error threshold.

4.4 Additional observations

While increasing the airspeed gradually from 0 to 15m/s, the aircraft starts oscillating heavily at a forward speed of 5m/s. The oscillations are mainly pitch oscillations, and it seems as if the back propellers are stalling and then recovering. This could be due to interaction between the front and back propellers. Even though the reason for this is still uncertain, it was easily mitigated by avoiding flying at that specific airspeed. In a mission for which this aircraft is designed, constantly flying at 5m/s is not a requirement.

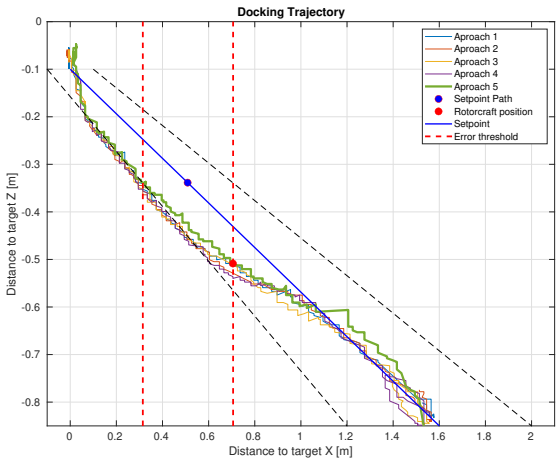

Figure 12: Path for 10 different approaches and setpoint position with respect to AC for the first aproach.

5 Conclusions & Recommendations

In conclusion, this scientific paper presents a proof of concept for rigid airborne docking using electromagnets between a fixed-wing aircraft and a hybrid rotorcraft. The successful demonstration of autonomous docking and undocking in a wind tunnel environment indicates the potential for future development and outdoor testing. The use of an INDI controller and horizontal motors for handling linear accelerations proved to be very effective and is recommended to be used in future work. The implemented cascaded proportional controller for position control, as well as the setpoint generation method used, yielded a smooth docking maneuver. The relative sensing method employing retroreflective ArUco markers and an infrared camera proved to work well in different lighting conditions. The methods presented in this paper should be tested in an outdoor environment with a real fixed-wing in future work. Overall, this study establishes the feasibility of rigid airborne docking and lays the groundwork for future advancements, holding promise for applications requiring precise docking between fixed-wing and rotorcraft vehicles.

References

[1] Nader S Labib, Matthias R Brust, Grégoire Danoy, and Pascal Bouvry. The rise of drones in internet of things: A survey on the evolution, prospects and challenges of unmanned aerial vehicles. *IEEE Access*, 9:115466–115487, 2021.

[2] Alessandro Bacchini, Enrico Cestino, Benjamin Van Magill, and Dries Verstraete. Impact of lift propeller drag on the performance of evtol lift+ cruise aircraft. *Aerospace Science and Technology*, 109:106429, 2021.

[3] Dylan O'Driscoll. Uavs in humanitarian relief and wider development contexts. 2017.

[4] Hoodtech Mechanical. Flying launch and recovery system. hoodtech-mechanical. Website, 06 2023.

[5] PS Ramesh and JV Muruga Lal Jeyan. Comparative analysis of fixed-wing, rotary-wing and hybrid mini unmanned aircraft systems (uas) from the applications perspective. *INCAS Bulletin*, 14(1):137–151, 2022.

[6] Mads Friis Bornebusch and Tor Arne Johansen. Autonomous recovery of a fixed-wing uav using a line suspended between two multirotor uavs. *IEEE Transactions on Aerospace and Electronic Systems*, 57(1):90–104, 2020.

[7] Kristian Klausen, Jostein Borgen Moe, Jonathan Cornel van den Hoorn, Alojz Gomola, Thor I Fossen, and Tor Arne Johansen. Coordinated control concept for recovery of a fixed-wing uav on a ship using a net carried by multirotor uavs. pages 964–973, 2016.

[8] Kristian Klausen, Thor I Fossen, and Tor Arne Johansen. Autonomous recovery of a fixed-wing uav using a net suspended by two multirotor uavs. *Journal of Field Robotics*, 35(5):717–731, 2018.

[9] Peter R Thomas, Ujjar Bhandari, Steve Bullock, Thomas S Richardson, and Jonathan L Du Bois. Advances in air to air refuelling. *Progress in Aerospace sciences*, 71:14–35, 2014.

[10] Daniel Briggs Wilson. Guidance, navigation and control for uav close formation flight and airborne docking. 2015.

[11] DARPA. Gremlins program demonstrates airborne recovery. Defense Projects, 05 2021.

[12] Inyeni Amakuro Showers et al. *Development of an autonomous airborne docking and undocking system for micro drones to a mother drone*. PhD thesis, Cape Peninsula University of Technology, 2019.

[13] Kevin Ling. Precision landing of a quadrotor uav on a moving target using low-cost sensors. Master's thesis, University of Waterloo, 2014.

[14] Alexandre Borowczyk, Duc-Tien Nguyen, André Phu-Van Nguyen, Dang Quang Nguyen, David Saussié, and Jerome Le Ny. Autonomous landing of a multirotor micro air vehicle on a high velocity ground vehicle. *Ifac-Papersonline*, 50(1):10488–10494, 2017.

[15] Ewoud JJ Smeur, Qiping Chu, and Guido CHE De Croon. Adaptive incremental nonlinear dynamic inversion for attitude control of micro air vehicles. *Journal of Guidance, Control, and Dynamics*, 39(3):450–461, 2016.

[16] Ewoud JJ Smeur, Guido CHE de Croon, and Qiping Chu. Cascaded incremental nonlinear dynamic inversion for mav disturbance rejection. *Control Engineering Practice*, 73:79–90, 2018.

[17] Muhammad Tahir, Sayed Saad Afzal, Muhammad Saad Chughtai, and Khurram Ali. On the accuracy of inter-vehicular range measurements using gnss observables in a cooperative framework. *IEEE Transactions on Intelligent Transportation Systems*, 20(2):682–691, 2018.

[18] Adam Marut, Konrad Wojtowicz, and Krzysztof Falkowski. Aruco markers pose estimation in uav landing aid system. In *2019 IEEE 5th International Workshop on Metrology for AeroSpace (MetroAeroSpace)*, pages 261–266. IEEE, 2019.

2

Additions

In this section, additions that were not included in the scientific article can be found.

2.1. Vision

In Figure 2.1, the NED relative position estimates are shown for both the vision system and the motion capture system, which is taken as the ”true” baseline. The rotorcraft is first commanded to stay 40cm behind and 25cm below the target and is then commanded some small deviations to see how well the vision system tracked the relative position. From the figure, we can see that the values are tracked well with no significant divergence. At just before 200 seconds and at 220 seconds, significantly fewer markers were in view, leading to higher deviations.

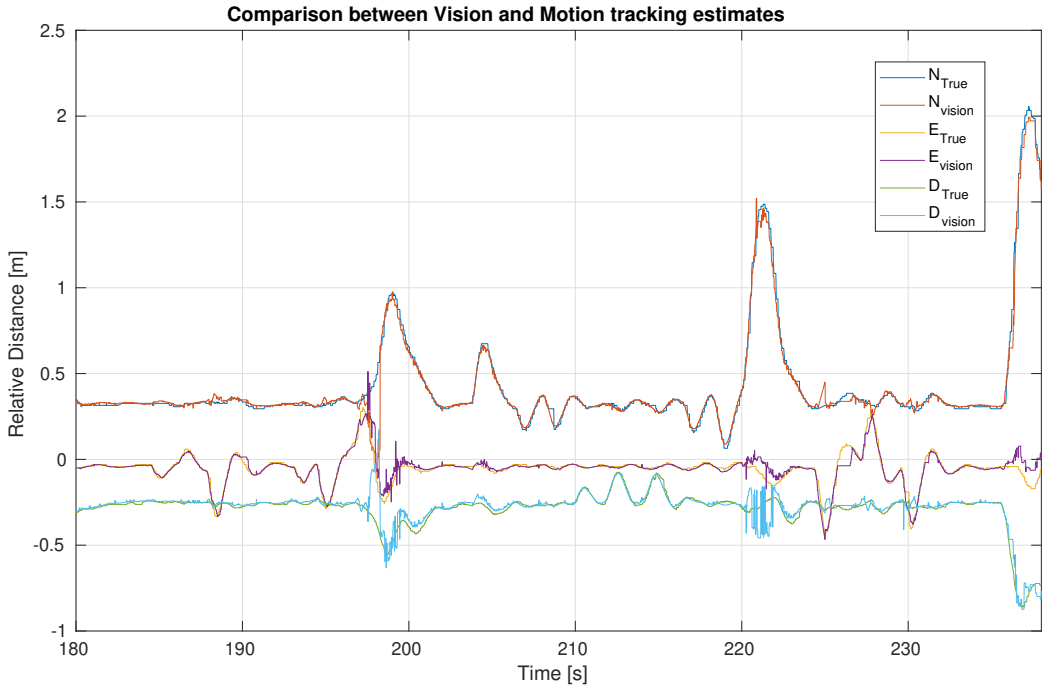

Figure 2.1: Comparison between OptiTrack and Vision

During the approach, a sequence of pictures was taken to show what the camera with the bandpass filter sees. This can be seen in Figure 2.2. Note that the detected markers are marked with a green line around their contour and their marker id is stamped by them.

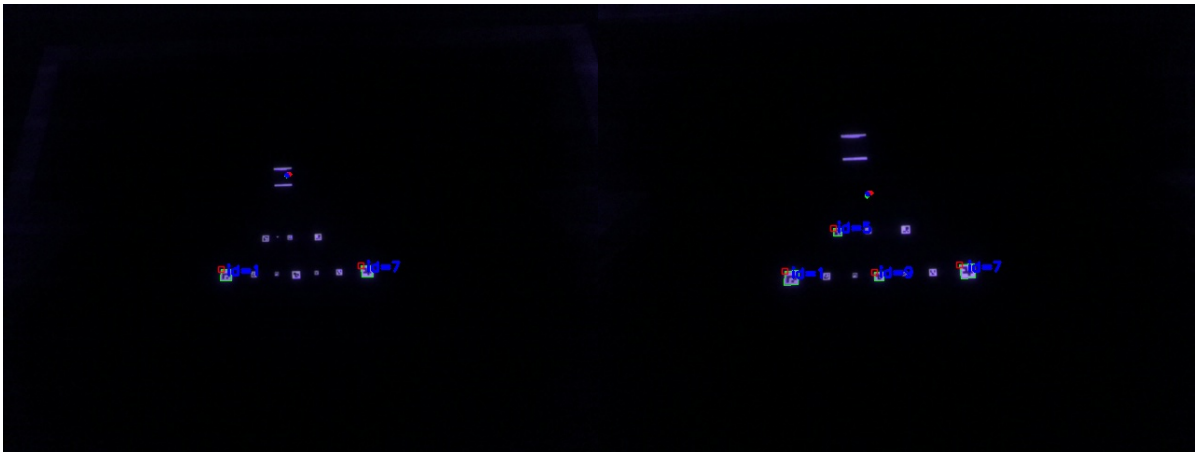

(a) 1 (b) 2

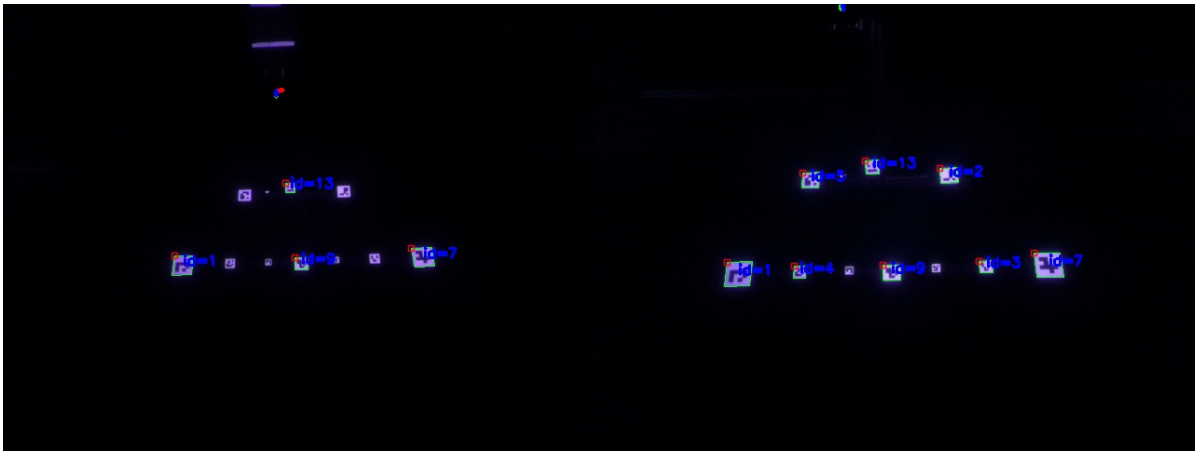

(c) 3 (d) 4

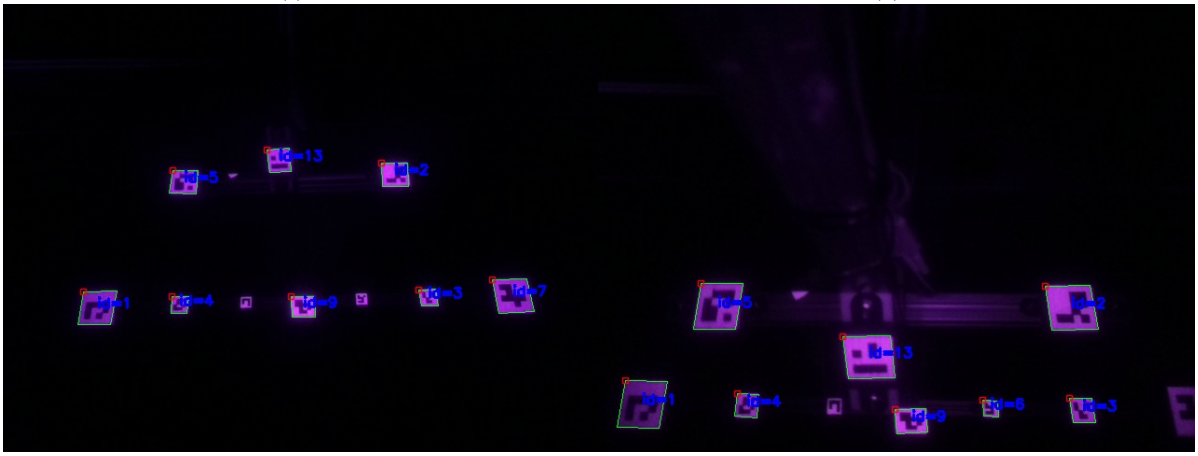

(e) 5 (f) 6

Figure 2.2: IR camera view during approach

2.2. Overactuated rotorcraft design

The manufactured lift rotorcraft can be clearly seen in Figure 2.3. This drone is an adaptation of an F350 drone frame, where the top and bottom plate (*1* and *2*) are re-designed, and 3D printed to accommodate the three lateral motors. A longer landing gear (*3*) was also made to allow the lateral rotors to spin without hitting the ground. Due to the lateral motors, stronger vibration can now be expected around all three axes. Passive damping is therefore included, where the camera and the flight controller are both suspended on a damped rubber platform (*4*). The docking hardware for the wind-tunnel demonstrations comprises a flat plate (*5*) that will attach the electro-magnets. A thickness of $3mm$ is chosen as it is a good compromise between pull force and mass. When operating the vehicle in the wind tunnel, the rope tethered to the drone is pushed back because of the incoming flow. To avoid it from getting tangled into the propellers, a simple propeller guard (*6*) was included. Note that the four downfacing propellers are in pusher configuration, to assure the necessary clearance for docking. Finally, the vision setup comprised of the four IR LEDs as well as the bandpass filter can be seen in (*7*). The design was made in such a way that all parts are easily replaceable to ensure little time loss when switching out broken parts after a crash.

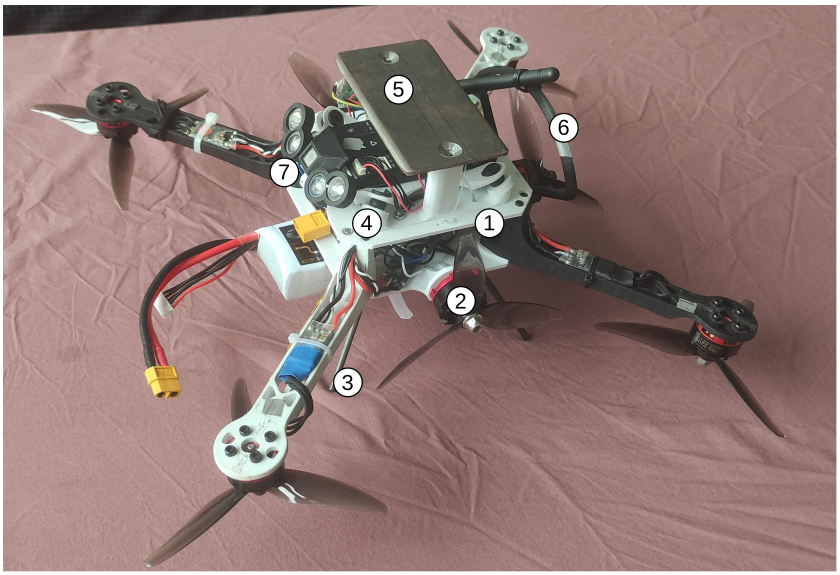

Figure 2.3: Overactuated rotorcraft

2.3. Setpoint Visualization

In the paper, the way the setpoint progresses forward is explained, but a series of figures were not shown. In Figure 2.4 a snapshot of the current aircraft position and its current reference position is seen at 6 different instances during the approach. A video of this can be seen in the youtube playlist[1] of this thesis project.

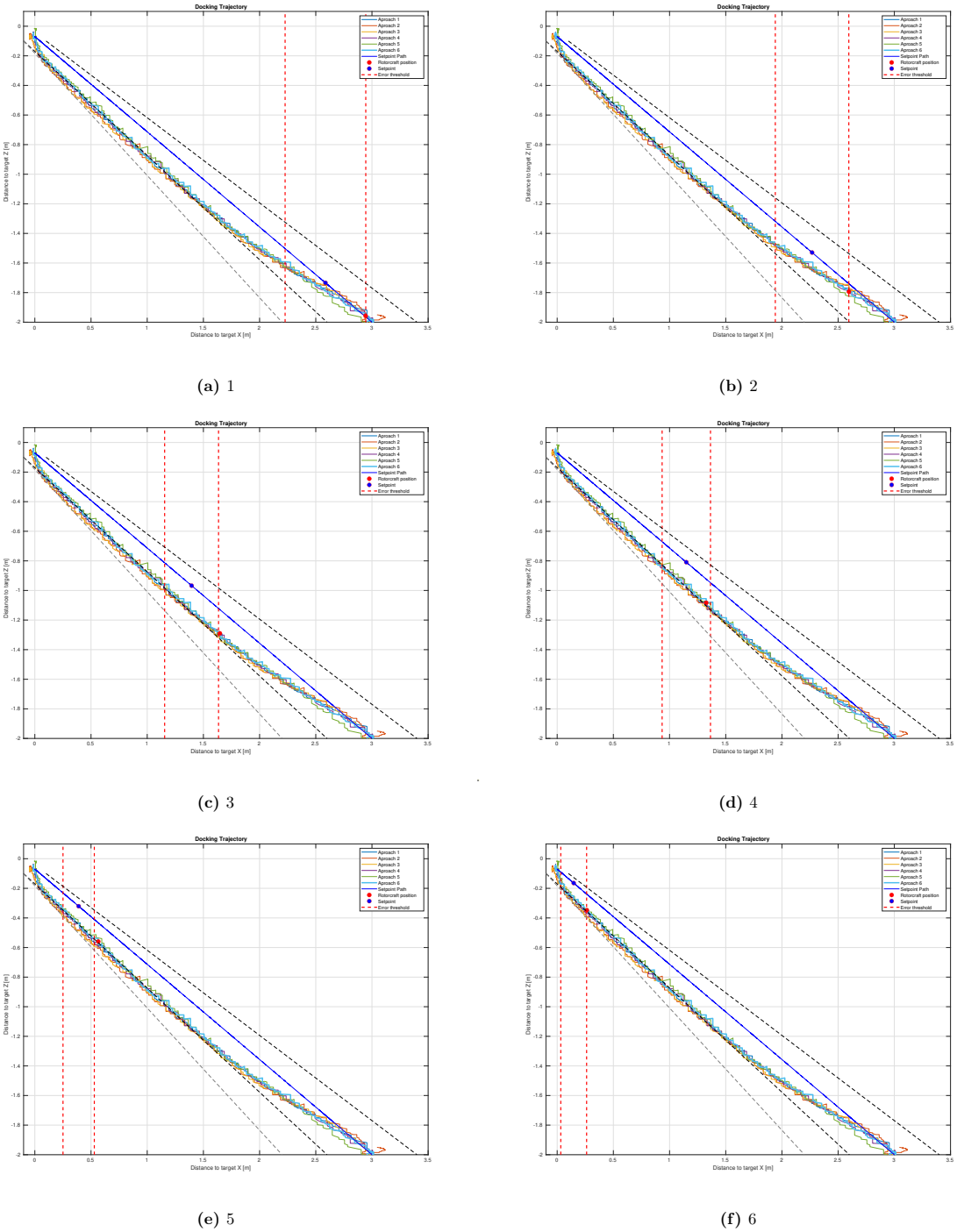

(a) 1 **(b)** 2

(c) 3 **(d)** 4

(e) 5 **(f)** 6

Figure 2.4: Visualization of setpoint advance and AC position

[1] https://www.youtube.com/playlist?list=PLGTkt2QO0hTnYZ0R1N5 Mrnp9tA1FefnFx

2.4. Recomendations for future work

Rigid docking was achieved to a static target in the wind tunnel at windspeeds of up to 14m/s. This is a good first step towards landing a fixed-wing UAV with rotorcraft and it validated the possibility to use electromagnets in conjunction with an overactuated platform. However, there are still a few steps to achieve the end goal:

Electromagnets were used as the docking mechanism in the experiments carried out. However, three electromagnets were placed in a line next to each other and a single flat plate was used, meaning there is only one attachment point. In future work leading to outdoor flights, it is recommended to use the electromagnets at three or four separated attachment points, to ensure correct position and orientation while docked, as well as to prevent unwanted separation due to a gust. Separate attachment points also allow for possible future additions like power delivery.

The author believes that fusing all sensor data to estimate relative position would be valuable as the vision would serve to update the estimates, allowing for the relative position error to degrade slowly when dropout occurs. This thesis focused on the development of the overactuated vehicle and the setpoint formulation, so there were no extensive efforts carried out to optimize the relative sensing method. There is a lot of room for improvement and it is recommended to investigate additional relative sensing methods. The relative position accuracy while both aircraft are solely on GPS for rendezvous must still be tested outdoors.

Once docked, a new challenge come to light. The two vehicles must land together. While one option could be to use a rotorcraft sized large enough to carry the fixed wing as dead weight, I believe it is better to have the two vehicles fly as a quadplane, and use the aerodynamic control surfaces as well as the fixed-wing engines during the transition and vertical flight. This becomes crucial if strong winds are present.

Part II

Literature Review

3

The need for airborne docking

3.1. Types of aircraft

The two main type of aircraft and their subcategories will now be discussed. Note that the focus is on miniature aerial vehicles.

3.1.1. Fixed wing aircraft

Fixed wing aircraft, as the name indicates it have wings that are "fixed" in place and generate their lift through the airflow generated by the forward velocity of the aircraft. Note that even though they are fixed, the wings are not necessarily rigid. Because the lift is generated by a forward velocity with respect to the air, these aircraft have a minimum airspeed, and hence required a solution for the transition from flying speeds to a halt, in which they cannot sustain flight. The general solution is in the form of a runway where the aircraft can touchdown at speeds close to the minimum airspeed, and slow down as it rolls, steadily decreasing the effect of the aerodynamic surfaces.

To decrease the needed length of such runway, one can either reduce the minimum flying speed or increase the braking performance on touch down. High lift devices, thrust reversal, parachutes and arresting cables are all solutions used nowadays in that objective.

The control of a conventional aircraft is achieved through the control of the engines and aerodynamic surfaces. Forward speed is controlled by the engines, roll is controlled with the ailerons, pitch through the elevator and yaw through the rudder. Of course, there are variations to this. Tailless aircraft such a flying wing, which are very common in the UAV sector use elevons, which combine the function of both elevators and ailerons. Yaw stability in most tailless aircraft is achieved through wing sweep and thrust differential can be used for yaw authority in the case that two or more engines are present.

3.1.2. Rotorcraft

Rotorcraft are vehicles that generate their lift by rotating a blade through the air, which then generates lift. Helicopters tend to have two or more rotors. Their placement and configuration depend on the type of helicopter, the standard being either coaxial, or a main rotor with a tail rotor. Control is achieved by the ability of the rotors to tilt or flap, creating variable thrust.

Multirotors are normally equiped with more than four rotors spaced equally from the centre of the frame. Using multiple rotors allows for the blades to have a fixed pitch, and control to be achieved by varying the thrust generated by the different motors. Increasing the number of rotors for fixed-size frame will allow for higher performance capabilities, at the cost of higher power consumption.

3.1.3. Hybrid aircraft

In the last few years there has been an increasing interest in the design of hybrid miniature UAVs. This can be associated with the increasing maturity and saturation of the conventional MAV industry, as well as the reduced barriers to development of hybrid alternatives. That is, there is already a vast amount of research and companies within the conventional rotorcraft/fixed-wing UAV industry, while there is much more space for research within the hybrid alternatives. At the same time, the costs to develop hybrid systems has decreased greatly due to cheaper and much more accessible components.

Hybrid UAVs are generally divided into two main families: convertiplane UAVs and Tailsitter UAVs. Convertiplane has a constant frame orientation both during forward and vertical flight, using different methods to transition from the different two flight modes. Tailsitters on the other hand, as their name indicates, take off and land vertically on its tail, and rotates the whole aircraft to achieve forward cruising flight.

In brief, convertiplane UAv's tend to have systems in place for the transition in the form of rotating rotors, rotating wings, or a very common dual system in which there are separate motors for forward and vertical flight. This leads to increased weight, complexity or increased drag, which all lead to poorer flight characteristics. Tail sitters on the other hand tend to be much harder to control and tend to be a lot more vulnerable to wind [3]. Due to the need for a thrust to weight ration higher than 1, all hybrid alternatives carry a propulsive system that is heavier than needed for efficient forward flight.

The additional drag sources resulting from hybridisation are discussed in [4] and the efficiency of the quadplane, the most common hybrid aircraft is compared in [5] with its fixed-wing counterpart. The drag polar obtained from experimental campaign comparing a mini Talon aircraft with its hybrid counterpart can be appreciated in Figure 3.1. The increase in drag alone is enough to move away from the quadplane alternative. Adding to that the disturbance of the flow downstream and the extra weight carried just for the VTOL phase makes a hybrid alternative less attractive. Mechanical systems to tackle the extra drag like retractable beams or rotating nacelles makes the aircraft heavier and increase the points of failure of the system. When VTOL in remote locations is not needed, and an airborne recovery solution can be used, airborne docking becomes an attractive solution.

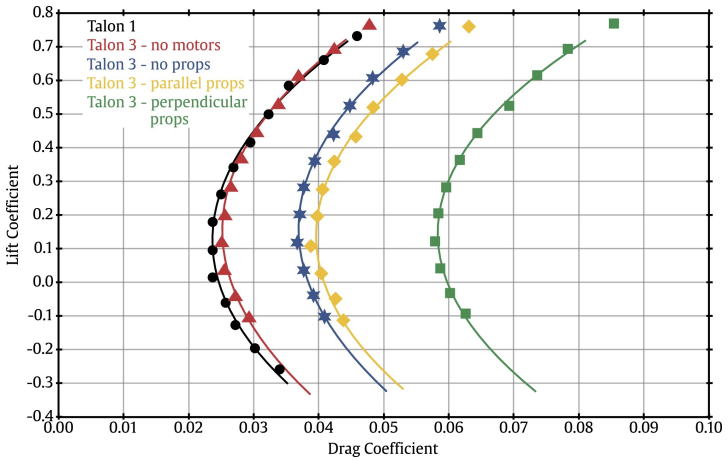

Figure 3.1: Drag Polar comparing a hybird alternative to a fixed wing aircraft

4

UAV Docking work & Docking Mechanisms

The clear benefit and need for airborne docking is presented in chapter 3. The advancements towards Airborne docking and the existing alternative solutions will now be discussed. Based on the available literature, three different docking approach are identified and named as follow: non-rigid, rigid and a hybrid alternative between the two. By non rigid, what is meant is the use of a system where the two vehicles are not rigidly joined post-docking. Consequently, Rigid docking is the use of rigid elements both during and post-docking. The hybrid alternative encompasses the systems were elements from rigid as well as non-rigid solutions are used. The three will now be discussed.

4.1. Non-Rigid Docking

Non-rigid docking generally involves an arresting system that the fixed wing aircraft goes into, typically rope based system like nets or arresting lines. The relative speeds of the two vehicles tend to be high and once docked, it is hardly possible to undo the manoeuvre. As it will be seen, this method requires less precise relative positioning, making it a cheap and robust alternative.

Zipline can be regarded as one of the first successful operational UAV delivery company. It started operating in rwanda in 2016. They have a conventional fixed wing airplane that is launched with a catapult from the central base. For recovery, Zipline uses a horizontal arresting cable that is suspended by two towers. The aircraft then hook onto it using a $1cm$ long tail hook. This approach, is reliable, robust to adverse meteorological conditions, and solves the inefficiencies of having a hybrid system. However, there is a need for infrastructure, and the base cannot be moved easily. Once captured, a human is still needed to recover the aircraft by hand before the line can be suspended again.

A similar approach is taken by *Hood Tech Mechanical* who, through various methods have the arresting wire placed vertically in tension. The hook of the aircraft is then be positioned at the extremities of the wings. A solution that is in use by Boeing and the U.S. Air-force, is a the patented *Sky Hook Recovery System* [6], which is composed of a line suspended between the ship's crane and a lower boom.A clip at the end of either wing of the aircraft captures the line. The rig can be replaced by a multi-copter pulling a tether vertically as can be seen in Figure 4.2. In this case, the arresting winch softens the impact.

Lastly, *Hood Tech Mechanical* are also offering a similar system where the tether is tensed between a parasail and a speedboat.[7] These variation of the same technique are effective against different weather conditions, and can be retrofitted to already flying UAVs. However, the system needs a tether in the ground since, as stated in their patent[8], sufficient rope tension and shock absorbing system was not achieved with a free rope. Additionally significant amount of infrastructure/equipment is needed, and the UAVs dock in a relatively violent manner, making it harder to scale to heavier aircraft. Once docked, a human operator must recover the aircraft that is hanging awkwardly on its side.

Figure 4.1: FLARES system on a boat

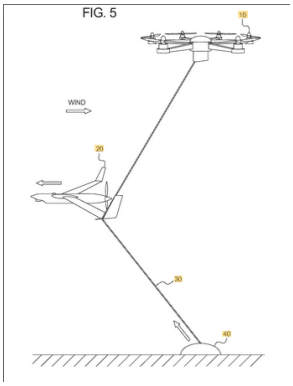

Figure 4.2: FLARES using a multicopter

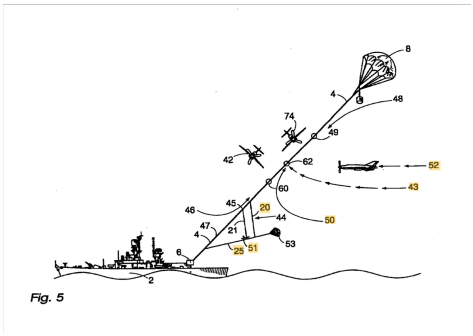

Figure 4.3: Parasail FLARES system[9]

All the systems that have been put forward try to land a fixed wing UAV without the need of a runway, but all fall short of a true airborne solution.

4.2. Hybrid Docking

Hybrid docking solutions are approaches for which elements of non-rigid docking the likes of ropes with drogues are used for first contact but the relative velocities of both vehicle are close to zero at docking. Therefore, the control problem becomes similar to that of rigid docking.

Towards the completion of his doctoral thesis, Wilson successfully had a fixed wing UAV to autonomously dock with a drogue towed by another UAV. This feat had not been previously demonstrated. In his work, Wilson tackles the challenges of needing highly accurate and reliable relative positioning performance amidst external disturbances by proposing, and experimentally verifying a guidance, navigation and control solution. His system augments the insufficient difference of individual UAV state estimates by fusing direct vehicle-to-vehicle observations. The use of IR markers as a visual direct relative measurement improves relative positioning, and the estimate accuracy degrades slowly when dropouts occur. The motion of the drogue was also derived, to propagate the dynamic model to the docking point. Using a general vector guidance strategy Brigs uncouples control and guidance allowing for this strategy to be used throughout all phases of the mission.Daniel's work on aircraft control terminal guidance will be discussed further in chapter 5.

In [10], Mads Friis et al. presents an airborne recovery system in which a stretched rope carried by two multicopters is used to intersect a line with a hook hanging from the fixed wing UAV. When the recovery is initiated, the fixed-wing UAV flies at a straight path with constant altitude that is called the virtual runway, while the multi-rotors ensure the relative positioning for a successful capture. At the time of capture, a mean error of 0.8m to the target position was achieved using RTK GPS. The recovery margins are dictated by the length of the hook line and horizontal catch line, which can easily be increased, making this recovery method very Robust. However, once caught, the UAV cannot be released, and is just dangling from the line, making human interaction needed for damage free recovery and relaunch.

This concept of using two multirotors has been investigated before with the use of a net instead instead of a line in [11] and then verified experimentally in [12]. The drawbacks of these methods were the increased weight of the net and the increased wind influence due to its bigger surface area. The wind sensitivity could be reduced by making the net smaller, at a cost of an increased need for accuracy. A net also increased the likelihood of damaging equipment protruding from the aircraft such as antennas, cameras, sensors, propellers, pitot-tubes, or any other. The need for an operator in ground is still needed to untangle assist for the recovery and untangling the UAV from the net. Needless to say this solution does not allow for undocking mid-flight.

On October 2021, Dynetics successfully recovered an X-61A aircraft using a towed drogue approach[13]. The system in action can be seen in Figure 4.4. While in the air, the operator sends the command for the X-61A to rendezvous with the recovery C-130. The UAV then proceeds to autonomously place itself and maintains its assigned position behind the C-130. When the engineering team in the control room is satisfied with the performance of the system, the UAV moves closer to the drogue flown below and

behind the C-130. Docking is finally commanded, and the system autonomously closes the final gap. Once docked, the drone shuts down its engines, folds its wings, and the recovery system reels the vehicle into the cargo bay. There is little published information about the project, as it is military research. However, it is stated that the disturbances created by the C-130 made the recoveries challenging and only one successful recovery was achieved.

Figure 4.4: Dynetics gremlin's recovery

Figure 4.5: Talyn concept

4.3. Rigid Docking

Rigid docking will be defined as a solution where rigid components are used for capture and post-docking. If achieved, this solution would be preferred for its lower impact on the air-frame, its comfort in the case of manned aircraft, and the ability to dock and separate mid-flight. While the need for a rigid solution is clear, there is no clear demonstration of it been used in forward flight. A few papers, mainly in the form of master theses attempt to tackle the topic with different concepts, but always fall short of a truly autonomous, forward flight docking solution.

A recent American startup called Talyn is designing a hybrid solution where a quadplane docks to a fixed-wing aircraft to land and take off. They patented the concept and are now working on development[14]. So far, no information is available about their control method, or mechanical docking solution. It is assumed that having a wing as well, the two vehicles would be affected by turbulence similarly, and therefore the need to actively compensate for it can be bypassed. This startup will be closely followed.

In his paper, Steven Lukow aimed to design and fabricate a prototype of an autonomous multirotor drone that can dock into a larger fixed-wing drone for Mars exploration[15]. Electromagnetic coils mounted on the fixed-wing drone were used to attach with neodymium magnets mounted on the top of both multirotors. The setup can be appreciated in Figure 4.6. When turned on, the electromagnetic coils become warm, allowing for a particularly good scenario for thermal imaging and guidance towards the docking points. There was no docking attempt

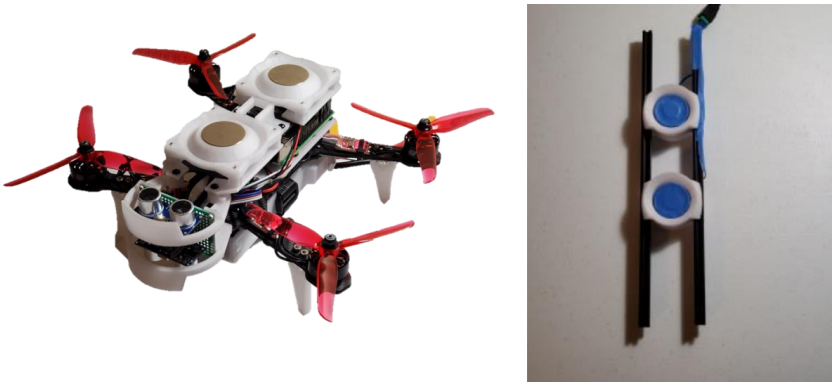

Figure 4.6: Docking system with electromagnets

In [16] the author uses a marker on an unmanned ground vehicle (UGV) to recognize the target and relative pose and land on it. The mission is devided in 3 segments, rendez-vous, then ensuring the target is being tracked properly and finally decent. Tests were done at very slow speeds, and the system

will become unstable at higher speeds. A architecture is used in [17], but this time with a gimballed camera that points towards the received location of the ground vehicle. Successful landing was achieved on a high speed ground vehicle traveling at 50km/h. Proportional navigation was used for rendez-vous, and PID for the terminal guidance. This will be discussed further in chapter 5.

5

Control Strategies, Rendez-vous, and Relative Guidance

Even-though flight stabilization, rendez-vous, formation flight and terminal guidance are different aspects of a mission, they often overlap, and regardless of the architecture, they always lead to the same sort of output: a scaled command on the actuators, in the form of motor RPM or control surface deflection. In section 5.2 and section 5.3, the flight stability and simple equations of motion of a fixed-wing aircraft and of a multi-copter will first be discussed. Then, various types of formation and terminal guidance will be discussed from section 5.4 on.

5.1. Reference frames

The reference frames most relevant to this study will now be mentioned briefly. The ones described are with respect to the navigation frame and can be seen in Figure 5.1. A more detailed approach can be found in [18].

The navigation coordinate frame is at the tangent plane to the earth surface. Also know as NED (north-east-down) the right-handed axes X,Y,Z point north, east and down respectively. When referring to the position of the follower, we use a coordinate frame where the origin is at the leader's COG. This will be mentioned as the navigation frame as it is the result of subtracting the follower's state from the leaders in the navigation frame.

The leader vehicle frame referred to as vehicle-1 frame in [19], has its origin at the COG of the leader vehicle and is rotated by $C_{(o,o,\psi)}$ to align the x axis with the vehicle's heading. It is used for relative motion between 2 vehicles.

The body frame has its origin at the COG of each vehicle and has its x-axis pointing towards the nose of the vehicle, the y-axis pointing towards the right and the z-axis towards the bottom of the aircraft. $C_{(\phi,\theta,\psi)}$ is the rotation matrix that rotates the navigation frame to the body frame.

The camera frame is used for visual navigation, has its origin at the camera's focal point, with X pointing to the right and Y pointing up with respect to the resulting image. Z then protrudes outwards from the focal point and is orthogonal to X and Y

The sensor frame has its origin at the inertial measurement unit and its axes are fixed to the component. The choice of the axis depend on the chosen configuration in software. This frame is used to account for sensor placement, and alignment with respect to other systems, which, if unaccounted for will lead to fatal propagated errors.

5.2. Control of a fixed-wing UAV

A conventional fixed-wing aircraft is controlled through its control surfaces (ailerons, elevator, and rudder) and throttle. Position control of such aircraft is generally split between lateral and longitudinal dynamics, as they can be assumed to be uncoupled. The control surfaces generate forces quadratically with airspeed, and hence body acceleration resulting from control surface deflection vary with airspeed.

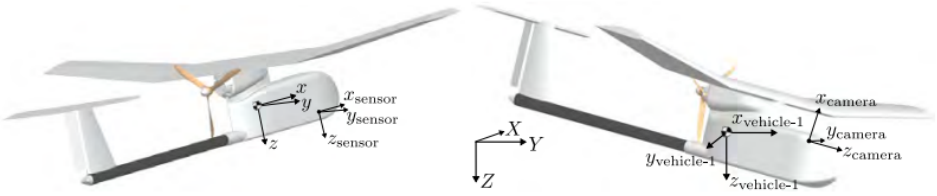

(a) Body frame and sensor frame. **(b)** Vehicle-1 frame and camera frame.

Figure 5.1: Coordinate frames described

Various control methods like gain scheduling can be used to tackle this as well as scaling those gains directly with airspeed [20].

Lateral control of such aircraft is achieved by controlling the bank angle, which is a result of aileron deflection. For airspeed and altitude control, it is not as simple. CHnaging the aircraft attitude will result in a change in height as well as airspeed. That is, kinetic energy was traded with potential energy. Increasing the throttle will increase the airspeed, which will create more lift, and hence also result in an increased height. Therefore, pitch angle and throttle both affect airspeed, which complicates the control problem. The conventional solution is in the form of a Total Energy Control System (TECS), which commands a throttle and pitch set-point. Thrust increases the total energy state of the aircraft which is the sum of potential and kinetic energies. While at a given total energy state, one can be flying high and slow, or low and fast. This is referred to as the specific energy balance it is controlled via the aircraft pitch angle. Increasing the pitch angle will covert kinetic to potential energy. [21] Poor pitch control will therefore affect the performance of airpseed/altitude tracking.

The attitude set-points are then sent to the fixed wing attitude controller which commands required angular accelerations. The attitude control of the PX4 system can be appreciated in Figure 5.2. This attitude controller uses a cascaded loop method. A rate set-point is generated by calculating the error between the estimated and desired attitude, and multiplying it with a gain. This P controller is then followed by an inner loop which uses PI control to achieve the desired angular accelerations. Note that a derivative term is not necessary due to aerodynamic damping. In fact, a feed forward term is used to compensate for it. The desired accelerations are then *mixed* to output a desired control surface deflection. Since lift is quadratic with respect to speed, the control surfaces are more effective at high speed and less effective at low speed. If an airspeed measurement is available, the the surface deflections can be scaled with it. The yaw controller generates its yaw rate set-point by minimizing lateral body acceleration, achieving coordinated turns.

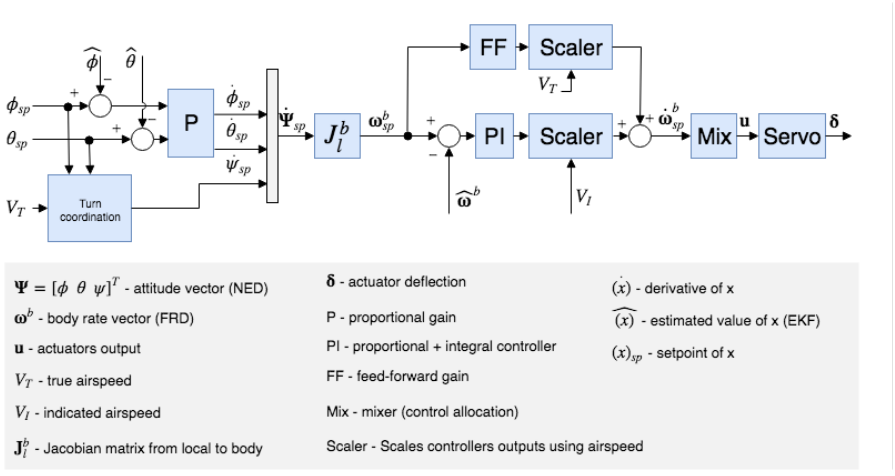

Figure 5.2: Attitude control loop [21]

5.3. Control of a multi-copter

Conventional multi-copters with downward facing rotors achieve control by varying the thrust of the individual motors. By having an equal amount of clockwise and anti-clockwise rotating motors, there are no resulting moments around Z on the air-frame. Yaw, pitch and roll angular accelerations are all controlled using differential angular speeds of the motors. Through this actuation, all the attitude or desired position of the drone can be achieved. There are various types of control strategies for both inner and outer loop stabilization, but all end up at the same type of output; a PWM value to the individual motors. A simplified diagram of the overarching control architecture of a conventional multi-copter can be seen in Figure 5.3. This is a cascaded controller where a position controller commands desired inertial accelerations. These inertial accelerations are then converted to desired attitude, which the attitude controller uses to command an angular rate. The desired rates are then passed by the rate controller to a "mixer" where the desired angular accelerations plus global thrust are translated to individual motor PWM values. The measured attitude and angular velocities are generally very noisy so filtering is needed before the controllers can use the data. In this case, which is the control architecture of *PX4*, the velocity and angular rate controllers are PID while position and angle are controlled by a simple proportional gain.

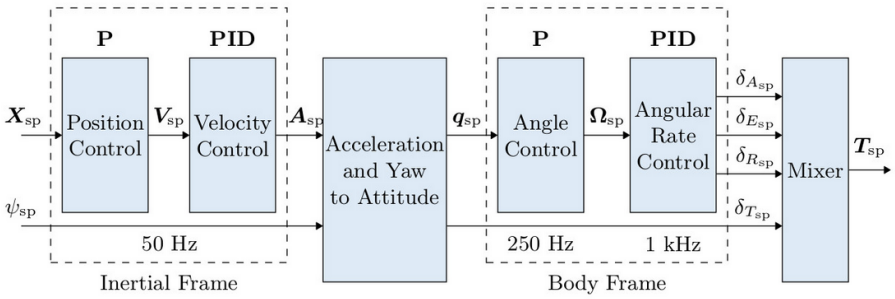

Figure 5.3: Simple representation of a conventional control structure [**?**]

PID (proportional-integral derivative) is one of the most common control systems amongst linear controllers due to its simplicity, ease of design, and ability to provide a satisfactory performance with relatively little control efforts. The main task in designing a PID controller is the proper selection or tuning of its gains. The proportional term K_p directly acts on the current error, the integral term K_i acts to minimize the accumulated past error, and the derivative term D_i acts to minimize the change of the error. Other inner loop stabilization techniques include LQR, which finds the optimal control between actuator effort and effectiveness [22], H+ intends to minimize response to disturbance and μ tries to compensate for varying disturbances[22]. There are many more control strategies, but since they often merge with higher level guidance commands, they will be discussed further if relevant to airborne docking.

5.4. Relative Guidance (Formation flight & Terminal guidance)

Formation flight as the name indicates it, takes place when two or more aircraft fly in a coordinate motion from a starting point to an ending one while maintaining a desired pattern. Anderson states that for a successful formation there must be two responsibilities; safely moving the formation as a whole from start to finish and maintain formation shape between agents during motion.

A typical formation controller block diagram that is found in literature can be appreciated in Figure 5.4. The system is made of two loops. The first (inner) loop, ensures local stabilization of the flight of the individual UAVs. The second (outer) one is tasked with achieving the desired formation by coupling UAV states, usually translational or rotational position or velocity, through a common control law and feeding its outputs as generated set-points for the inner loop[23].

There is a lot of research on formation guidance so the focus will be kept on dual-vehicle formation. The approaches can be identified as synchronised, pursuit based or state based. Synchronised formation is a simple approach where two vehicles follow the same trajectory. It goes without saying that this leads to relative accuracy too low for airborne docking. This synchronised approach was shown in [24]

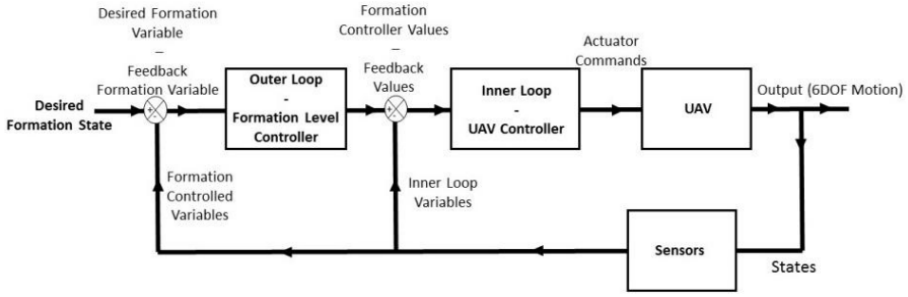

Figure 5.4: Typical formation controller block diagram

and [25], the latter shortening the formation distance up to 12m.

5.4.1. Pursuit based strategies

The missile guidance literature has motivated the use of pursuit based strategies for airborne UAV encounters. Three types of guidance laws are identified: line of sight (LOS), pursuit guidance and proportional navigation.

LOS guidance ensures the missile remains in the line of sight between the launching site and the target. A common and simple type of this method is called Beam Riding, in which the target is illuminated with a radio, laser or radar beam and the missile control system ensures it remains in the centre of said beam. This method needs a direct line of sight between the base and target and leads to high lateral accelerations in the final phase[26]. Since this method is of no relevant use in the scope of this thesis, it will not be discussed further. Pursuit guidance aims to nullify the relative LOS angle between the vehicle and the target. This method follows a similar path to LOS guidance and is generally further split into body pursuit and velocity pursuit, the difference being that velocity pursuit aims to point the velocity vector of the missile at the target instead of the longitudinal axis. By mounting the "seeker" of the missile to a vane, the angle between the velocity vector and LOS to the target can directly be measured without the need of much computational effort. Just like LOS guidance, this method leads to high lateral acceleration requirements towards the terminal phase and often leads to a tail chase. This method is often referred to as LOS guidance in academia even-though in pursuit guidance, it is the vehicle that is tracking the target. Work in [27], [28] and [29] use this method by calculating the LOS angle from cameras on-board. Experiments show that while useful and robust for rendez-vous and distant formation, this method tends to become unstable at close distance[30]. To minimize the effect, a discrete gain scheduling technique is proposed in [28].

A popular and heavily used guidance algorithm is proportional navigation guidance. In this method, the angular rate of the missile is kept proportional to the rate of change of the vehicle-to-target vector. The proportional navigation constant is then the ratio between the missile turning rate and the LOS rate of change and is typically between 2 and 5. There are many variations to proportional navigation such as in [31] and [32] were the distance to the target is used in the control law directly to attempt to mitigate the unstable behavior at small separations.

5.4.2. Setpoint-based guidance strategies

Setpoint guidance strategies aims to minimize the offset between the vehicle and a commanded fomration setpoint, which is generally rigidly joined to the leader as can be seen in [33], [34] and [35]. While this strategy does perform better, accurately estimating the relative states of the vehicle is the challenge and it will be discussed in chapter 6. Additionally, when the leader turns, the setpoints suddenly become very large due to the rotating frame. Wilson's work solves that problem by augmenting the setpoint state to account for leader turn dynamics [19]. In his work, his terminal guidance algorithm calculates the setpoint position based on the alignment error. This effectively creates a funnel that leads to the drogue. As stated before, it is estimating the relative error that is the most complicated. Once achieved, various control methods can be used to minimize this errorsuch as linear quadratic regulation [34] and synthesised PID controllers[35]. Wilson uses a vector based guidance technique which decouples control from guidance[36]. This will be further explored in section 5.5

5.5. Vector Guidance

In his work, Wilson develops a vector based-guidance strategy which minimizes error between the setpoint state P_s and V_s and the current state P and V by controlling the bank angle ϕ_{cmd} for lateral control, airspeed $v_{a_{cmd}}$ for longitudinal control and vertical velocity $V_{Z_{cmd}}$ for vertical control. With this technique, the guidance can be decoupled and it is the setpoint formulation that defines the mission. Such method is illustrated in Figure 5.5. As we can see, the commanded velocity vector V_{cmd} is the addition of the setpoint velocity with the commanded closing velocity $V_{s|c_{cmd}}$. This closing velocity is the distance between P_S and P multiplied by a horizontal and vertical gain $K_{P_{XY}}$ and K_{P_Z} respectively. The commanded yaw rate is then calculated by directly feeding forward the setpoint rotation rate to maintain alignment and adding it to the angle between V_{cmd} and V with a proportional gain K_{P_ϵ}.

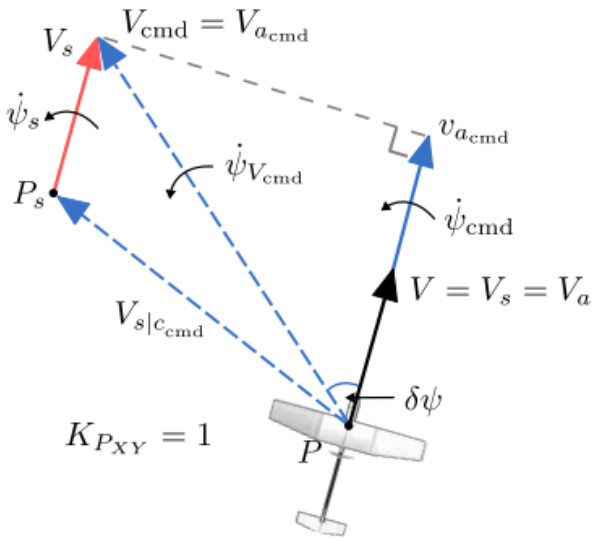

Figure 5.5: A 2D illustration of the vector guidance used to transition to, and maintain, a setpoint state. Wind is assumed to be zero. [19]

5.5.1. Setpoint formulation for Formation and Terminal guidance

As stated previously, the input of the vector guidance control is setpoint position P_s, setpoint velocity V_s, and $\dot{\psi}$ which is the setpoint rotation rate of V_s. These parameters are derived from the desired formation configuration and the leader's state as will be shown in this section.

The formation configuration P_{cmd} is given as a point in "leader vehicle frame". A typical close formation configuration where the follower vehicle trails the leader by 3 meters is given by: $P_{cmd} = [X_{cmd}\ Y_{cmd}\ Z_{cmd}]^T = [-3\ 0\ 0]^T$. However, this setpoint must first be augmented to compensate for wind and leader turn dynamics.

The commanded formation is first rotated by the crab angle to be in the direction of the inertial velocity v_l as seen in Figure 5.6. This leads to a commanded X_{cmd} and Y_{cmd} with respect to the heading of the path. This is important, as in the case of turn, this means that a different arc must be made by the follower to maintain formation as can be seen is Figure 5.7. To find the characteristics of the arc, the rate of change of the leader's heading $\dot{\boldsymbol{\psi}}_{\boldsymbol{l}}$ must first be found. Instead of differentiating ψ_l the instantaneous value can be found using Equation 5.1, where the leader's gyro rate measurement is used directly after being corrected for the effect of wind. More detail can be found in [19]

$$\dot{\boldsymbol{\Psi}}_{\boldsymbol{l}} = \dot{\psi}_l \cos\left(\psi_l - \boldsymbol{\Psi}_{\boldsymbol{l}}\right) \frac{V_{a_l}}{V_l} \tag{5.1}$$

The turn radius r , angle θ and Length R can then be easily calculated using Equation 5.2,Equation 5.3 and Equation 5.4 respectively. Note that in straight flight, $R = \bar{X}_{cmd}$

$$r = \frac{V_l}{\dot{\Psi}_l} \tag{5.2}$$

$$\theta = \frac{\bar{X}_{cmd}}{r} \tag{5.3}$$

$$R = 2r \sin\frac{\theta}{2} \tag{5.4}$$

The augmented setpoint position P_s can now be calculated using Equation 5.5, where the chord R is rotated by $\theta/2$ and $\bar{Y}_{cmd}$ by θ. The final rotation of $\boldsymbol{\psi_l}$ converts the results to the navigation frame.

$$P_s = C_{(0,0,\Psi)} \left(C_{(0,0,\frac{\theta}{2})} \begin{bmatrix} R \\ 0 \\ \bar{Z}_{cmd} \end{bmatrix}^T + C_{(0,0,\theta)} \begin{bmatrix} 0 \\ \bar{Y}_{cmd} \\ 0 \end{bmatrix}^T \right) + P_l \tag{5.5}$$

Since the rotation rate of the leader and follower must be the same, the magnitude of the desired velocity setpoint V_S can be derived as seen in Equation 5.6. Finally, this velocity setpoint must tangent to the path at setpoint position P_S, which is done by rotating the normalized leader velocity by θ, and scaling it by the previously found setpoint speed, as shown in Equation 5.7. Now that all required setpoint states are formulated, the vector guidance can be used. An overview of the overarching result can be appreciated in Figure 5.8.

$$\dot{\boldsymbol{\Psi}}_{\boldsymbol{l}} = \frac{V_S}{r - \bar{Y}_{cmd}} = \frac{V_l}{r} \quad \Longrightarrow \quad V_s = V_l - \bar{Y}_{cmd}\dot{\boldsymbol{\Psi}}_{\boldsymbol{l}} \tag{5.6}$$

$$V_s = V_s C_{(0,0,\theta)} \frac{V_l}{V_l} \tag{5.7}$$

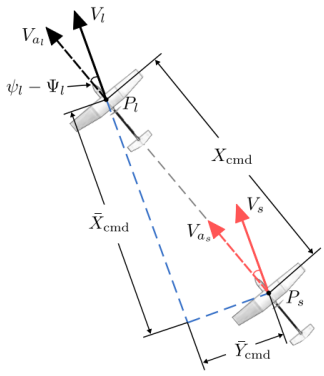

Figure 5.6: Relative position augmentation to account for wind

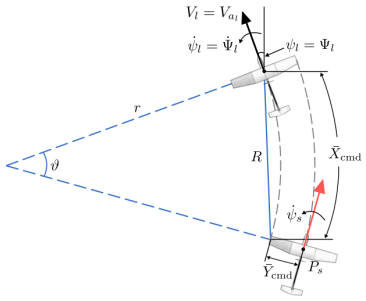

Figure 5.7: Setpoint state during banked turns

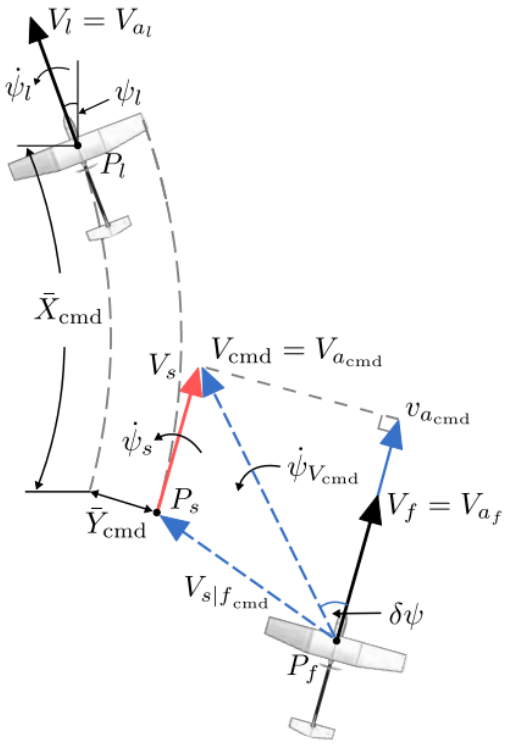

Figure 5.8: 2D illustration of the vector guidance in combination with the formulated setpoint state during banked turns

6

Sensing

Small UAVs bring forward difficult sensing requirement due to various reasons. To begin, micro-air-vehicles tend to have fast dynamics and require real-time feedback to be controllable. The size of these also restricts payload mass and volume. To achieve precise relative position control, one must first accurately estimate the relative position and pose, which makes the sensing challenge all the more difficult. This chapter will give an overview of the relative sensing methods used nowadays.

6.1. Differencing global position

Estimating the relative state of a vehicle with respect to another one can be done by measuring directly, or by subtracting the position measurements taken by each individual vehicle's onboard sensors. The problem with this approach, is that a communication link between UAVs is required, the time at which the data was taken must be accounted for, and measurement inaccuracies of each vehicle add up towards the total inaccuracy of the system. That is why solely differencing GNSS is not sufficient for close proximity flight [37][38]. Even-though GNSS measurements are partially correlated since the signal from each satellite are subject to the same atmospheric conditions, reception of different satellites will cause the error to be less correlated. One can mitigate this by ensuring that the position estimate of both vehicles is calculated using the same satellites[39]. This however computational adds delay to the system and multi-path make it so that relative position is often in excess of 5m[36]. Dual frequency GPS can suppress multi-path error [40] and the use of various constellation also ensure more satellites are available at once, reducing dropouts in accuracy[41]. GNSS data can be post processed and improved by using known atmospheric attenuation from bases around the world, and real time kinematic (RTK) gps significantly improves the relative state accuracy real time, but a fixed-base is needed, and can therefore hardly be used on a mobile vessel. It is important to note that accuracy degrades in dynamic environments. Using UWB ranging between the two vehicles in addition to GNSS/INS, has shown to improve a degradation in accuracy due to phase breaks in dynamic environments[42][43][44]. It is however generally accepted, that GNSS based sensing methods must be supported by more precise means of relative sensing.

The use of ultra-wideband tags is seeing an increased use due to their simplicity and ability to be used in GNSS denied environments. They also do not rely on objects being in the field of view of the sensor, like is the case for cameras. They are often used with anchors of know location[45]. In [46] 2 vehicles with 4 tags and 2 tags respectively were able to estimate their relative pose with a RMS error of 10cm at a relative range of 10m. In [46] 2 tags were used to achieve a relative pose error of 0.75m and 3degrees. UWB tags are promising, specially for bigger UAV, were the tags can be positioned further apart.

6.2. Vision

Visual sensors remain the go to sensor for precise relative positioning for their cheap price, small form factor, ease to integrate, and their potential given the advancements in computer vision. Visual based sensors can be categorized into three main orientations: monocular vision, stereo vision and active sensing devices such as LIDAR and Radar[47].

Active methods emit power and sense the resulting incoming signals. Light detection and ranging (LiDAR) sensors illuminate a target and measures the distance by analyzing the reflected light. These sensors can provide a wide field of view and are highly accurate. However, their size nad cost make them problematic for smaller UAV use[48]. Radars continuously emit electromagnetic waves and detect an obstacle when the emitted waves are reflected back towards it. The distance is then calculated though the time difference between the emitted and reflected wave. While radar has a wider sensing range than LIDAR and can scan an area quickly, LIDAR has a higher accuracy and resolution, allowing for a 3D model generation of the illuminated target [49]. 3D Lidar has shown to be a viable solution in [50], in which the point cloud generated by the sensor was matched with a 3d model of a tanker, achieving 40cm accuracy. Work in [51] shows advancements in this method, achieving 17cm accuracy. While lidar for 1d ranging have become widely available, their 3D counterparts as still too power intensive and heavy for their use in small UAVs.

Given that stereo vision and active sensors tend to be less flexible in their use, and less advantageous in terms of mass, operational range, processing power and power consumption, a lot of effort has been put into the research of monocular vision.[52]. This is specially due to the rapid pose estimation possible with lower mass and power requirements[53]. Monocular vision translates the observed information from the camera frame into the 3D environment through various methods. Defining monocular vision as the use of a single visual sensor, three distinctions in the type of sensor can be made. CCD/CMOS are used to obtain an image and is what is present in most cameras. They are sensitive to the visible spectrum and the near visible infrared, often fitted with a filter to shield from the noise caused by this NIR radiation. The research done in computer vision uses this type of sensor and will further be discussed. Dynamic Vision Sensors also known as event cameras output a perceived change in brightness instead of the momentary image allowing for smaller latency. Andrea Censi et al. used this sensor to detect active LED markers that are fixed to a UAV and modulated at individual frequencies[54]. While this allowed for rapid detection and identification of the markers and subsequently UAV pose, once attached to a moving vehicle, the camera quickly becomes cluttered with outliers. Another type of sensor are the elctro-optical sensors which detect direction of incident light. A notable example is the VisNav sensor developed for spacecrfat relative navigation, in which area Position Sensing Diode (PSD) photodetectors in the focal plane of a camera are used to detect the direct line of sight angle from incoming active LED markers[55].This technology has started being applied in UAV relative navigation [56] and Air to air refueling in [57],[58]. An extension of this system called "iVisNav" is proposed, where the time derivative of the phase shift of the modulated markers is used to estimate rotational rates as well[59].

Monocular vision using CMOS/CCD sensors use featureless or feature based approaches. Featureless approaches use the aircraft shape and centroid to estimate relative pose. Template matching attempts to find the best match between the captured image and a predefined library of aircraft at different poses. A Centre Only Relative State Estimation (CORSE) algorithm in [60] uses the centroid of the captured image and the inertial information of the follower estimate the relative state. To calculate the range to the target, the follower must take a sinusoidal flight path. A different technique called Subtended Angle Relative State Estimation(SARSE) tackles this problem by using the wingtips to estimate the range. In [61] and [62] these methods are demonstrated in real life.

Feature based methods are more popular, where features of the aircraft are identified and then matched to known models of the aircraft. This can be either passive, using features such as corners in the image or and active methods like optical markers. [52] gives a detailed overview of the different methods to identify and track the pose of an uncooperative vehicle as well as their effectiveness in different lighting conditions, which is one of the biggest challenges.

In [27], Darling implemented airborne relative pose estimation using visual LED markers and the Efficient Perspective-n-Point (EPnP) pose estimation algorithm. Wilson then continued on this work achieving airborne-docking between a fixed-wing aircraft and a drogue using IR LED markers. The use of IR LEDs saw a notable increase in use, notably in [63] where a pyramid configuration of camera's is used to estimate the relative position between the sensor and active markers using amplitude modulated infrared light. This insect-based sensor can measure azimuth and elevation angles with respect to two small and cheap active IR LEDs flickering at two different frequencies. In [64], an IR camera with a 100 Hz update rate is used to calculate the range and bearing to IR LED markers onboard another UAV. A root mean square error of 4.65cm is achieved. A similar approach is done in [65] where different marker configurations for different UAVs allow for relative pose estimation as well as identification of individual agents in a swarm.

7

Electromagnets

Given that electromagnets will be used as docking mechanisms, a brief overview of the magnetic properties will be discussed.

7.1. Existing hardware

The company Nicadrone developed the OpenGrab EPM v3 which is an Electro Permanent Magnet gripper capable of holding about 15kg of cargo securely. AS opposed to a pure electromagnet, the magnetic force to grip the ferromagnetic object come from a permanent magnet within. Releasing of the cargo is then accomplished by delivering a short pulse to an electromagnet which reverses it's field. Magnetic interference is discussed, on the ardupilot user guide for this hardware, and it is recommended to check the magnetic field values while turning on the device. A change of 10% is deemed acceptable. It is recommended to place the device more than $10cm$ away from the flight controller.

7.2. Force of an electromagnet

The holding force of a magnet is defined as the force (in kg) needed to separate it from a steel plate. Given that air is not permeable the pull force of a magnet is shown to decreases with the air gap in a cubic manner. Thin plates do not adhere well as permeability is smaller causing the magnetic field to saturate [66]. The pull strength is strongest at areas with the strongest changing magnetic field, which in turn depend on the shape of the magnet. In [67] 4 pyramid shaped magnets are joined to create a much stronger magnetic beam, and hence, a stronger pull force at larger distances. The pull force between 2 magnets in contact is the same as the pull force between one of the magnets and a steel plate. However, when separated, the pull force between the two magnets will degrade slower than with a steel-magnet combination[68].

Bibliography

[1] Nader S Labib, Matthias R Brust, Grégoire Danoy, and Pascal Bouvry. The rise of drones in internet of things: A survey on the evolution, prospects and challenges of unmanned aerial vehicles. *IEEE Access*, 9:115466–115487, 2021.

[2] Alessandro Bacchini, Enrico Cestino, Benjamin Van Magill, and Dries Verstraete. Impact of lift propeller drag on the performance of evtol lift+ cruise aircraft. *Aerospace Science and Technology*, 109:106429, 2021.

[3] Adnan S Saeed, Ahmad Bani Younes, Chenxiao Cai, and Guowei Cai. A survey of hybrid unmanned aerial vehicles. *Progress in Aerospace Sciences*, 98:91–105, 2018.

[4] Alwin R Wang and Towen Chan. Estimation of drag for a quadplane hybrid unmanned aerial vehicle. In *AIAA Student Region VII Conference*, pages 5–11, 2017.

[5] Alessandro Bacchini, Enrico Cestino, Benjamin Van Magill, and Dries Verstraete. Impact of lift propeller drag on the performance of evtol lift+ cruise aircraft. *Aerospace Science and Technology*, 109:106429, 2021.

[6] Erin Moreland, Michael Cameron, Robyn Angliss, and Peter Boveng. Evaluation of a ship-based unoccupied aircraft system (uas) for surveys of spotted and ribbon seals in the bering sea pack ice. *Journal of Unmanned Vehicle Systems*, 3:114–122, 09 2015.

[7] Flares system vtol.

[8] Us9656765b2 - helicopter-mediated system and method for launching and retrieving an aircraft - google patents.

[9] William R McDonnell. Launch and recovery system for unmanned aerial vehicles, Aug 2014.

[10] Mads Friis Bornebusch and Tor Arne Johansen. Autonomous recovery of a fixed-wing uav using a line suspended between two multirotor uavs. *IEEE Transactions on Aerospace and Electronic Systems*, 57(1):90–104, 2020.

[11] Kristian Klausen, Jostein Borgen Moe, Jonathan Cornel van den Hoorn, Alojz Gomola, Thor I Fossen, and Tor Arne Johansen. Coordinated control concept for recovery of a fixed-wing uav on a ship using a net carried by multirotor uavs. In *2016 International Conference on Unmanned Aircraft Systems (ICUAS)*, pages 964–973. IEEE, 2016.

[12] Kristian Klausen, Thor I Fossen, and Tor Arne Johansen. Autonomous recovery of a fixed-wing uav using a net suspended by two multirotor uavs. *Journal of Field Robotics*, 35(5):717–731, 2018.

[13] Dynetics | gremlins air vehicles the road to airborne recovery.

[14] James Gull and Evan Mucasey. Vehicle, system, and method for vertical take-off and landing, Mar 2022.

[15] Inyeni Amakuro Showers et al. *Development of an autonomous airborne docking and undocking system for micro drones to a mother drone*. PhD thesis, Cape Peninsula University of Technology, 2019.

[16] Kevin Ling. Precision landing of a quadrotor uav on a moving target using low-cost sensors. Master's thesis, University of Waterloo, 2014.

[17] Alexandre Borowczyk, Duc Tien Nguyen, André Phu-Van Nguyen, Dang Quang Nguyen, David Saussié, and Jerome Le Ny. Autonomous landing of a multirotor micro air vehicle on a high velocity ground vehicle. volume 50, pages 10488–10494. Elsevier B.V., 7 2017.

[18] Randal W Beard and Timothy W McLain. Small unmanned aircraft. In *Small Unmanned Aircraft*. Princeton university press, 2012.

[19] Daniel Briggs Wilson, Ali Haydar Göktoğan, Salah Sukkarieh, Daniel B Wilson, and Ali H Göktoˇgökto ˇgan. Guidance and navigation for uav airborne docking. 2015.

[20] Pakorn Poksawat, Liuping Wang, and Abdulghani Mohamed. Gain scheduled attitude control of fixed-wing uav with automatic controller tuning. *IEEE Transactions on Control Systems Technology*, 26(4):1192–1203, 2018.

[21] Controller diagrams | px4 user guide.

[22] Sherif I Abdelmaksoud, Musa Mailah, and Ayman M Abdallah. Control strategies and novel techniques for autonomous rotorcraft unmanned aerial vehicles: A review. *IEEE Access*, 8:195142–195169, 2020.

[23] Brian D.O. Anderson, Bariş Fidan, Changbin Yu, and Dirk Van Der Walle. Uav formation control: Theory and application. *Lecture Notes in Control and Information Sciences*, 371:15–33, 2008.

[24] Zouhair Mahboubi, Zico Kolter, Tao Wang, and Geoff Bower. Camera based localization for autonomous uav formation flight. In *Infotech@ Aerospace 2011*, page 1658. 2011.

[25] Sanghyuk Park, John Deyst, and Jonathan How. A new nonlinear guidance logic for trajectory tracking. In *AIAA guidance, navigation, and control conference and exhibit*, page 4900, 2004.

[26] George M Siouris. *Missile guidance and control systems*. Springer Science & Business Media, 2004.

[27] Michael B Darling. *Autonomous close formation flight of small UAVs using vision-based localization*. PhD thesis, Cal Poly, 2014.

[28] Joseph W Nichols, Liang Sun, Randal W Beard, and Timothy McLain. Aerial rendezvous of small unmanned aircraft using a passive towed cable system. *Journal of Guidance, Control, and Dynamics*, 37(4):1131–1142, 2014.

[29] Min-Jea Tahk, Chang-Su Park, and Chang-Kyung Ryoo. Line-of-sight guidance laws for formation flight. *Journal of Guidance, Control, and Dynamics*, 28(4):708–716, 2005.

[30] DB Wilson and AH Goktogan. An unmanned aerial vehicle rendezvous and formation. In *Proceedings of the 2012 International Conference on Unmanned Aircraft Systems (ICUAS'12)*, 2012.

[31] Amir Betser, Patricio Vela, and Allen Tannenbaum. Automatic tracking of flying vehicles using geodesic snakes and kalman filtering. In *2004 43rd IEEE Conference on Decision and Control (CDC)(IEEE Cat. No. 04CH37601)*, volume 2, pages 1649–1654. IEEE, 2004.

[32] Yoshimasa Ochi and Takeshi Kominami. Flight control for automatic aerial refueling via png and los angle control. In *AIAA guidance, navigation, and control conference and exhibit*, page 6268, 2005.

[33] Jovan D Boskovic, Sai-Ming Li, and Raman K Mehra. Semi-globally stable formation flight control design in three dimensions. In *Proceedings of the 40th IEEE Conference on Decision and Control (Cat. No. 01CH37228)*, volume 2, pages 1059–1064. IEEE, 2001.

[34] Fabrizio Giulietti, Lorenzo Pollini, and Mario Innocenti. Autonomous formation flight. *IEEE Control Systems Magazine*, 20(6):34–44, 2000.

[35] James K Hall and Meir Pachter. Formation maneuvers in three dimensions. In *Proceedings of the 39th IEEE Conference on Decision and Control (Cat. No. 00CH37187)*, volume 1, pages 364–369. IEEE, 2000.

[36] Daniel Briggs Wilson. Guidance, navigation and control for uav close formation flight and airborne docking, 2015.

[37] Omead Amidi. *An autonomous vision-guided helicopter*. Carnegie Mellon University, 1996.

[38] Arthur Barfield and Jacob Hinchman. An equivalent model for uav automated aerial refueling research. In *AIAA Modeling and Simulation Technologies Conference and Exhibit*, page 6006, 2005.

[39] Muhammad Tahir, Sayed Saad Afzal, Muhammad Saad Chughtai, and Khurram Ali. On the accuracy of inter-vehicular range measurements using gnss observables in a cooperative framework. *IEEE Transactions on Intelligent Transportation Systems*, 20(2):682–691, 2019.

[40] Jason N Gross, Yu Gu, and Matthew B Rhudy. Robust uav relative navigation with dgps, ins, and peer-to-peer radio ranging. *IEEE Transactions on Automation Science and Engineering*, 12(3):935–944, 2015.

[41] Michael E. Hodgson. On the accuracy of low-cost dual-frequency gnss network receivers and reference data. *GIScience & Remote Sensing*, 57(7):907–923, 2020.

[42] Jason N. Gross, Yu Gu, and Matthew B. Rhudy. Robust uav relative navigation with dgps, ins, and peer-to-peer radio ranging. *IEEE Transactions on Automation Science and Engineering*, 12(3):935–944, 2015.

[43] Yuhang Jiang, Mark Petovello, and Kyle O'Keefe. Augmentation of carrier-phase dgps with uwb ranges for relative vehicle positioning. In *Proceedings of the 25th International Technical Meeting of The Satellite Division of the Institute of Navigation (ION GNSS 2012)*, pages 1568–1579, 2012.

[44] Yang Qi, Yisheng Zhong, and Zongying Shi. Cooperative 3-d relative localization for uav swarm by fusing uwb with imu and gps. In *Journal of Physics: Conference Series*, volume 1642, page 012028. IOP Publishing, 2020.

[45] Anton Ledergerber, Michael Hamer, and Raffaello D'Andrea. A robot self-localization system using one-way ultra-wideband communication. In *2015 IEEE/RSJ International Conference on Intelligent Robots and Systems (IROS)*, pages 3131–3137. IEEE, 2015.

[46] Ehab Ghanem, Kyle O'Keefe, and Richard Klukas. Testing vehicle-to-vehicle relative position and attitude estimation using multiple uwb ranging. In *2020 IEEE 92nd Vehicular Technology Conference (VTC2020-Fall)*, pages 1–5, 2020.

[47] Yuebo Ma, Rujin Zhao, Enhai Liu, Zhuang Zhang, and Kun Yan. A novel method for measuring drogue-uav relative pose in autonomous aerial refueling based on monocular vision. *IEEE Access*, 7:139653–139667, 2019.

[48] Eulalia Balestrieri, Pasquale Daponte, Luca De Vito, and Francesco Lamonaca. Sensors and measurements for unmanned systems: An overview. *Sensors*, 21(4):1518, 2021.

[49] B Nikhil Chand, P Mahalakshmi, and VPS Naidu. Sense and avoid technology in unmanned aerial vehicles: A review. In *2017 International Conference on Electrical, Electronics, Communication, Computer, and Optimization Techniques (ICEECCOT)*, pages 512–517. IEEE, 2017.

[50] Joseph Curro, John Raquet, Thomas Pestak, Jared Kresge, and Mark Smearcheck. Automated aerial refueling position estimation using a scanning lidar. In *Proceedings of the 25th International Technical Meeting of the Satellite Division of The Institute of Navigation (ION GNSS 2012)*, pages 774–782, 2012.

[51] Michael R Crowl. Use of lidar in automated aerial refueling to improve stereo vision systems. 2020.

[52] Lorenzo Pasqualetto Cassinis, Robert Fonod, and Eberhard Gill. Review of the robustness and applicability of monocular pose estimation systems for relative navigation with an uncooperative spacecraft. *Progress in Aerospace Sciences*, 110:100548, 2019.

[53] Sumant Sharma, Jacopo Ventura, and Simone D'Amico. Robust model-based monocular pose initialization for noncooperative spacecraft rendezvous. *Journal of Spacecraft and Rockets*, 55(6):1414–1429, 2018.

[54] Andrea Censi, Jonas Strubel, Christian Brandli, Tobi Delbruck, and Davide Scaramuzza. Low-latency localization by active led markers tracking using a dynamic vision sensor. In *2013 IEEE/RSJ international conference on intelligent robots and systems*, pages 891–898. IEEE, 2013.

[55] John Junkins, Declan Hughes, Karim Wazni, and Vatee Pariyapong. Vision-based navigation for rendezvous, docking and proximity operations. 101, 01 2002.

[56] Adam M Fosbury and John L Crassidis. Relative navigation of air vehicles. *Journal of Guidance, Control, and Dynamics*, 31(4):824–834, 2008.

[57] Monish D Tandale, Roshawn Bowers, and John Valasek. Trajectory tracking controller for vision-based probe and drogue autonomous aerial refueling. *Journal of Guidance, Control, and Dynamics*, 29(4):846–857, 2006.

[58] John Valasek, Kiran Gunnam, Jennifer Kimmett, Monish D Tandale, John L Junkins, and Declan Hughes. Vision-based sensor and navigation system for autonomous air refueling. *Journal of Guidance, Control, and Dynamics*, 28(5):979–989, 2005.

[59] Kookjin Sung, Ramchander Bhaskara, and Manoranjan Majji. Interferometric vision-based navigation sensor for autonomous proximity operation. In *2020 AIAA/IEEE 39th Digital Avionics Systems Conference (DASC)*, pages 1–7, 2020.

[60] EN Johnson, Y Watanabe, J Ha, AJ Calise, and AR Tannenbaum. Image processor, estimation, guidance, and flight test of vision-based formation flight. In *Proceedings of the 3rd International Symposium on Innovative Aerial/Space Flyer Systems*, 2006.

[61] Eric N Johnson, Anthony J Calise, Yoko Watanabe, Jincheol Ha, and James C Neidhoefer. Real-time vision-based relative aircraft navigation. *Journal of Aerospace Computing, Information, and Communication*, 4(4):707–738, 2007.

[62] Yoko Watanabe. *Stochastically optimized monocular vision-based navigation and guidance*. Georgia Institute of Technology, 2008.

[63] Thibaut Raharijaona, Rodolphe Mawonou, Thanh Vu Nguyen, Fabien Colonnier, Marc Boyron, Julien Diperi, and Stéphane Viollet. Local positioning system using flickering infrared leds. *Sensors*, 17(11), 2017.

[64] Mark Cutler, Bernard Michini, and Jonathan P How. Lightweight infrared sensing for relative navigation of quadrotors. In *2013 International Conference on Unmanned Aircraft Systems (ICUAS)*, pages 1156–1164. IEEE, 2013.

[65] Xudong Yan, Heng Deng, and Quan Quan. Active infrared coded target design and pose estimation for multiple objects. In *2019 IEEE/RSJ International Conference on Intelligent Robots and Systems (IROS)*, pages 6885–6890. IEEE, 2019.

[66] Yoshikazu Ishikawa and Sōshin Chikazumi. Design of high power electromagnets. *Japanese Journal of Applied Physics*, 1(3):155–173, mar 1962.

[67] Lockheed martin corp, 1999. apparatus and method for amplifying a magnetic beam. us5929732a.

[68] Francis Bitter. The design of powerful electromagnets part ii. the magnetizing coil. *Review of Scientific Instruments*, 7(12):482–488, 1936.